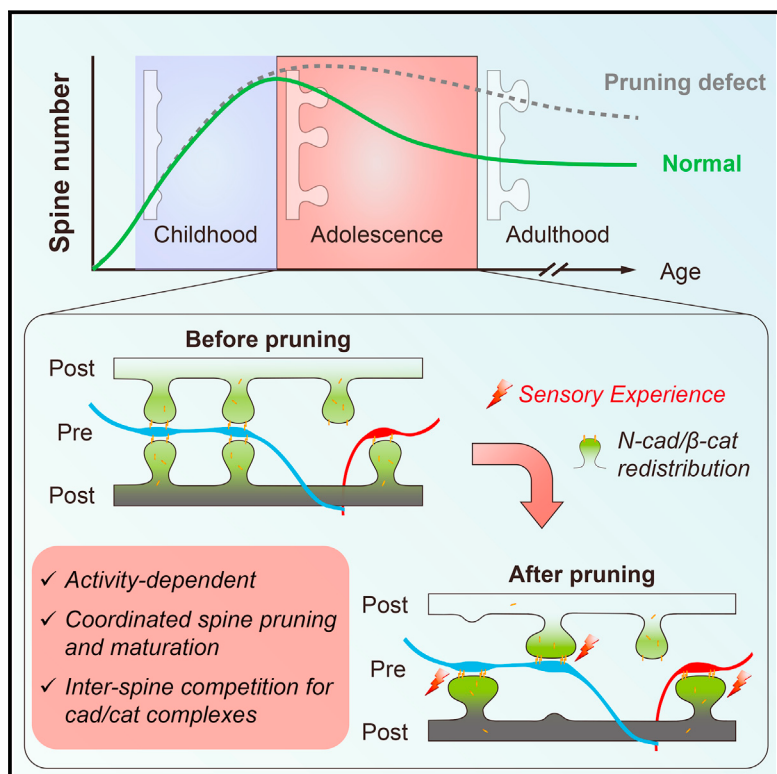


Coordinated Spine Pruning and Maturation Mediated by Inter-Spine Competition for Cadherin/Catenin Complexes

Graphical Abstract



Authors

Wen-Jie Bian, Wan-Ying Miao, Shun-Ji He, Zilong Qiu, Xiang Yu

Correspondence

yuxiang@ion.ac.cn

In Brief

The pruning or elimination of dendritic spines is always coordinated with the maturation of surviving neighboring spines. This process is bidirectionally regulated by neural activity and mediated by inter-spine competition for cadherin/catenin cell adhesion complexes.

Highlights

- Spine pruning and maturation in the mammalian brain are coordinated events
- Competition for cadherins and catenins mediates spine maturation and elimination
- Inter-spine competition for β -catenin *in vivo* biases spine fate during pruning
- Activity-dependent acceleration of spine pruning and maturation requires β -catenin



Coordinated Spine Pruning and Maturation Mediated by Inter-Spine Competition for Cadherin/Catenin Complexes

Wen-Jie Bian,^{1,2} Wan-Ying Miao,¹ Shun-Ji He,¹ Zilong Qiu,¹ and Xiang Yu^{1,*}

¹Institute of Neuroscience, State Key Laboratory of Neuroscience, CAS Center for Excellence in Brain Science, Shanghai Institutes for Biological Sciences, Chinese Academy of Sciences, Shanghai 200031, China

²University of Chinese Academy of Sciences, Beijing 100049, China

*Correspondence: yuxiang@ion.ac.cn

<http://dx.doi.org/10.1016/j.cell.2015.07.018>

SUMMARY

Dendritic spines are postsynaptic compartments of excitatory synapses that undergo dynamic changes during development, including rapid spinogenesis in early postnatal life and significant pruning during adolescence. Spine pruning defects have been implicated in developmental neurological disorders such as autism, yet much remains to be uncovered regarding its molecular mechanism. Here, we show that spine pruning and maturation in the mouse somatosensory cortex are coordinated via the cadherin/catenin cell adhesion complex and bidirectionally regulated by sensory experience. We further demonstrate that locally enhancing cadherin/catenin-dependent adhesion or photo-stimulating a contacting channelrhodopsin-expressing axon stabilized the manipulated spine and eliminated its neighbors, an effect requiring cadherin/catenin-dependent adhesion. Importantly, we show that differential cadherin/catenin-dependent adhesion between neighboring spines biased spine fate in vivo. These results suggest that activity-induced inter-spine competition for β -catenin provides specificity for concurrent spine maturation and elimination and thus is critical for the molecular control of spine pruning during neural circuit refinement.

INTRODUCTION

By virtue of their bulbous heads and constricted necks (Cajal, 1911), dendritic spines provide important biochemical and electrical compartmentalization within neurons, housing the postsynaptic density of excitatory synapses and associated organelles (Harris and Weinberg, 2012; Higley and Sabatini, 2012; Murakoshi and Yasuda, 2012; Sheng and Kim, 2011; Yuste, 2013). Previous studies demonstrated that rapid spinogenesis during early postnatal life (McAllister, 2007; Tada and Sheng, 2006; Yuste and Bonhoeffer, 2004) is followed by significant reduction in spine density during the transition through adoles-

cence, suggesting substantial synapse/spine pruning (Elston et al., 2009; Huttenlocher, 2002; Rakic et al., 1986, 1994). In vivo imaging in the mouse sensory cortices further demonstrated that during brain maturation, the rate of spine elimination substantially exceeded that of spine formation (Grutzendler et al., 2002; Holtmaat et al., 2005; Zuo et al., 2005a). This high rate of spine elimination, together with its regulation by sensory experience (Trachtenberg et al., 2002; Xu et al., 2009; Yang et al., 2009; Zuo et al., 2005b), suggested that the pruning of existing connections between neurons likely serve as an important process in the refinement of neural circuits (Alvarez and Sabatini, 2007; Bhatt et al., 2009; Fu and Zuo, 2011; Holtmaat and Svoboda, 2009).

In addition to dynamics in number, spines also show diversity in morphology, with thin spines being more motile and mushroom spines being more stable and containing larger postsynaptic densities (Harris et al., 1992; Holtmaat et al., 2005; Zuo et al., 2005a). Local increase in neural activity or induction of long-term potentiation (LTP) has been shown to induce the formation of new spines and/or the enlargement of existing spines, while spine shrinkage is associated with long-term depression (LTD) (Engert and Bonhoeffer, 1999; Maletic-Savatic et al., 1999; Matsuzaki et al., 2004; Murakoshi and Yasuda, 2012; Nagerl et al., 2004; Zhou et al., 2004). Based on these observations, it has been proposed that new spines (mostly thin) underlie memory acquisition, while stable spines (mostly mushroom and stubby) contribute to memory consolidation and storage (Bourne and Harris, 2007; Kasai et al., 2003).

The total excitatory input of a neuron is determined by the combined parameters of spine density and spine size/shape. Interestingly, while activity-dependent changes in spine density and shape have been extensively investigated independently (Alvarez and Sabatini, 2007; Bhatt et al., 2009; Bourne and Harris, 2008; Harris et al., 1992; Holtmaat and Svoboda, 2009; Segal, 2005; Spacek and Harris, 1997; Tada and Sheng, 2006), they have rarely been examined simultaneously in the context of spine pruning. Furthermore, since spine pruning during adolescence is temporally and phenotypically distinct from the degenerative and global loss of spines due to aging or pathological disorders such as Alzheimer's disease (Penzes et al., 2011; Sheng et al., 2012), different molecular mechanisms are likely to be employed. Importantly, in post-mortem human samples and animal models of neurodevelopmental disorders, including autism

spectrum disorders (ASD), intellectual disability, and schizophrenia, alterations in spine density and/or shape, possibly attributing to defects in spine pruning, have been reported (Glausier and Lewis, 2013; He and Portera-Cailliau, 2013; Penzes et al., 2011; Tang et al., 2014; Zoghbi and Bear, 2012). Thus, identification of mediators of spine pruning is critical to our understanding of the mechanism underlying neural circuit refinement.

Since neural activity is a driving force in development, we first investigated the effect of sensory experience on spine density and maturation. We found highly correlated, experience-dependent spine pruning and maturation in the mouse primary somatosensory cortex. Using live imaging, we further demonstrated that locally elevating neural activity or cadherin/catenin-dependent cell adhesion led to enlargement of the stimulated spine and concurrent pruning of its neighbor, an effect dependent on inter-spine distance and N-cadherin motility. Furthermore, selective enrichment of β -catenin in a small proportion of spines in vivo through pre-synaptic manipulations promoted the survival and maturation of β -catenin-enriched spines, at the expense of neighboring spines with lower β -catenin levels. Finally and importantly, acceleration of spine pruning induced by environmental enrichment was abolished in the absence of endogenous β -catenin. Together, these results demonstrate a critical role of the cadherin/catenin complex in mediating coordinated spine pruning and maturation during neural circuit refinement.

RESULTS

Activity-Dependent Spine Pruning in the Maturing Brain

We used environmental enrichment from birth (EE), a paradigm that increased sensory stimulation via multiple modalities (He et al., 2010; Zheng et al., 2014), to investigate the *in vivo* effects of neural activity on spine density and morphology over the developmental period of 1 to 3 months (m). Using Golgi staining, we found significant reduction in spine density in basal dendrites of layer 2/3 pyramidal neurons in the barrel field of the primary somatosensory cortex (S1BF), the primary motor cortex (M1), the piriform cortex (Pir), and the primary visual cortex (V1), as well as in medium spiny neurons of the dorsal striatum (CPu), both in mice reared under control and enriched conditions (Figures 1A, 1B, and S1A–S1D). These results suggest that spine pruning is a general phenomenon occurring in multiple sensory/motor regions, as the organism matures from adolescence to adulthood. Interestingly, brain regions primarily thought to be responsible for learning and memory, including the prefrontal cortex (PFC) and the hippocampal CA1 region, demonstrated complex changes in spine density over this period, suggesting that they either did not undergo spine pruning at the population level or did so with different time courses (Figures S1E and S1F). This difference may reflect requirement of the hippocampus and PFC to learn throughout life, rather than en masse within a critical period (Hensch, 2004), as is typical for sensory and motor cortices.

Of brain regions undergoing spine pruning, S1BF demonstrated the most striking developmental- and activity-dependence. In control mice, the reduction in spine density was most significant between 2 and 3 m, while in EE-reared mice, it was completed between the younger age of 1 and 2 m, despite

significantly elevated spinogenesis before 1 m (Figures 1B and S1G). The enrichment-induced acceleration of spine pruning was specific to basal dendrites of layer 2/3 pyramidal neurons (Figures 1B and S1H–S1J), which mostly receive within-column excitatory inputs from layer 4 and layer 2/3 neurons (Petersen, 2007). Based on these observations, we focused on spines on the basal dendrites of S1 layer 2/3 neurons.

To assess developmental changes in spine maturation, we classified the spines into four categories according to their morphology (Harris et al., 1992; Zagrebsky et al., 2005), under the general understanding that mushroom and stubby spines represented more mature spines, while thin and branched spines tended to be more plastic and immature (Bourne and Harris, 2008; Harris et al., 1992; Spacek and Harris, 1997; Tada and Sheng, 2006). We found that the proportion of mature spines increased with age, a process accelerated by EE-rearing (Figure 1C). We note that this acceleration of spine maturation temporally coincided with that of spine pruning, suggesting the EE-rearing effects on spine maturation and pruning were coordinated. Importantly, we observed a significant inverse correlation between the percentage of mature spines (mushroom and stubby spines) and spine density for all data from Ctrl and EE mice (Figure 1D, $R^2 = 0.30$, $p < 0.0001$). We note that at 3 m, spines from EE-reared mice were more clustered (Govindarajan et al., 2006; Kleindienst et al., 2011; Larkum and Nevian, 2008), as demonstrated by a shift of the distribution to shorter inter-spine distances (Figure 1E). The mature spines from EE-reared mice were also bigger (Figure 1F, see also Figure 7C). These results are similar to the effects of motor learning (Fu et al., 2012) and ocular dominance shift (Chen et al., 2012) and consistent with potentially increased synaptic strength and/or more refined local circuitry in EE-reared mice.

To investigate whether sensory experience was required for spine pruning, we trimmed one side of the whiskers in mice reared under standard conditions from 2 to 3 m. While significant spine pruning and maturation occurred over this period in the ipsilateral S1BF, corresponding to the intact whiskers, both processes were effectively blocked in the contralateral cortex, corresponding to the trimmed whiskers (Figures 1G–1J). Thus, spine pruning and maturation in S1BF occurred concurrently and are bidirectionally regulated by sensory experience through the whiskers, demonstrating tight coupling between these processes.

A Requirement for the Cadherin/Catenin Complex in Spine Pruning

The above observations suggested a model in which neural activity locally induced differentiation of spine fates, with some spines being eliminated while others matured. We hypothesize that this fate differentiation is mediated by redistribution of limited resources with the following characteristics: (1) enriched in spines, (2) regulated by neural activity, and (3) “motile” and redistributable between spines. Synaptic cell adhesion molecules fulfill all criteria, with the added advantage of being trans-synaptic and thus capable of coordinating pre- and post-synaptic changes (Giagtzoglou et al., 2009; Hirano and Takeichi, 2012; Südhof, 2008). We started by testing important cell adhesion molecules identified in post-synaptic densities, namely N-cadherin and β -catenin (Sheng and Kim, 2011). N-cadherin is a

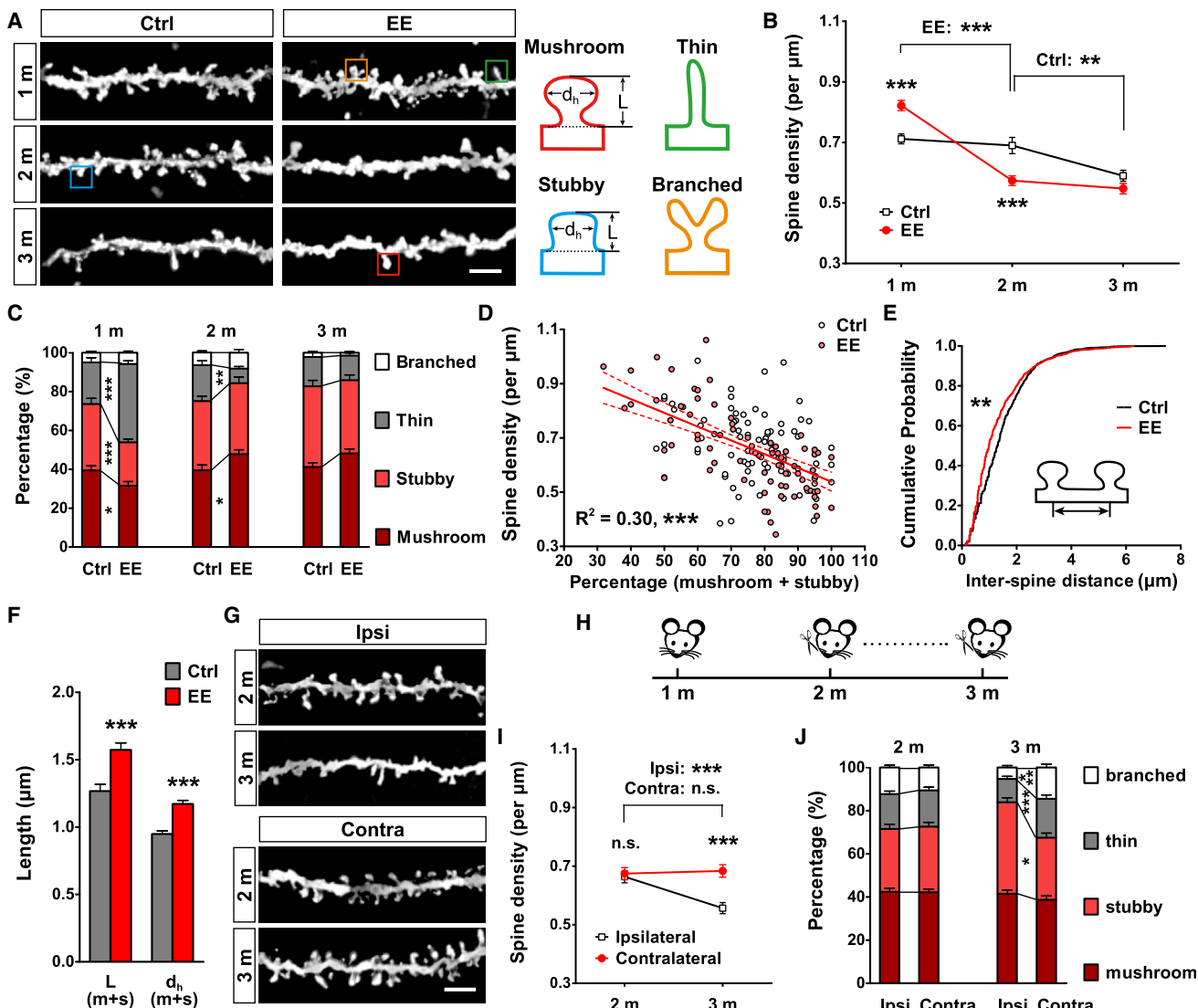


Figure 1. Activity-Dependent Spine Pruning in S1BF

(A) Representative inverted Golgi staining images showing spines in basal dendrites of layer 2/3 pyramidal neurons in S1BF, categorized as mushroom (red), stubby (blue), thin (green), and branched (orange) subtypes.

(B and C) EE accelerated spine pruning (B, n = 30–50/group) and maturation (C) in S1BF.

(D) An inverse correlation between spine density and the percentage of mature spines from all data in (B) and (C) (n = 155, R² = 0.30, p < 0.001).

(E) Cumulative distribution of inter-spine distances in Ctrl and EE mice at 3 m (n = 975, 950 segments in Ctrl, EE, p = 0.001).

(F) The length and head diameter of mushroom and stubby spines were increased in EE mice at 3 m (n = 169, 179 spines in Ctrl, EE).

(G and H) Representative inverted Golgi staining images showing spines in S1BF (G) and whisker deprivation protocol (H).

(I and J) Whisker deprivation blocked spine pruning (I, n = 36–40/group) and maturation (J) in contralateral S1BF.

Scale bars, 5 μm. Data are presented as mean ± SEM. In this and all subsequent figures, *p < 0.05; **p < 0.01; ***p < 0.001; n.s.: p > 0.05. See also Figure S1.

homophilic, calcium-dependent transmembrane cell adhesion molecule present at high levels pre- and post-synaptically. Together with its intracellular binding partners β-catenin and αN-catenin, it forms the cadherin/catenin complex, which has been shown to play important roles in synapse formation and plasticity (Arikath and Reichardt, 2008; Benson and Huntley, 2012; Brigidi and Bamji, 2011; Hirano and Takeichi, 2012; Tai et al., 2008). To investigate requirement for the cadherin/catenin complex in spine pruning in vivo, we conditionally knocked out

endogenous β-catenin in excitatory neurons of the cerebral cortex and hippocampus using inducible CaMKCreERT2 (β-cat^{f/f}; CaMKCreERT2^{+/−}; β-cat cKO) from 1 m, after the peak of synaptogenesis (Figures S2A–S2F). By 3 m, β-cat cKO mice had significantly higher spine density (Figures 2A and 2B) as well as less mature spines (Figure 2C), as compared with LoxP littermates (β-cat^{f/f}; LoxP Ctrl), suggesting impaired spine pruning and maturation. These concurrent defects were very similar to the effects of whisker trimming (Figures 1G–1J), suggesting a

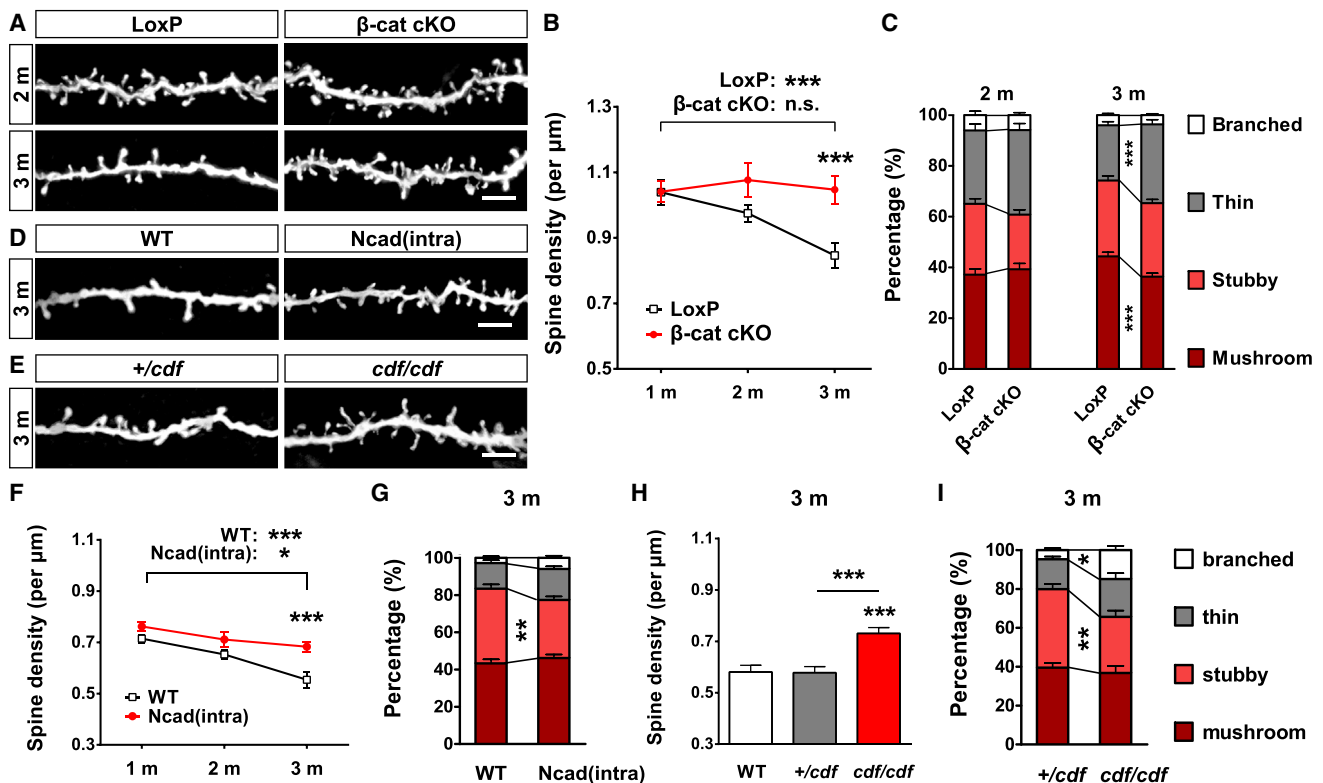


Figure 2. Appropriate Spine Pruning and Maturation Require the Cadherin/Catenin Complex

(A) Representative inverted Golgi staining images of spines in S1BF of $\beta\text{-cat}^{fl/fl}$; $\text{CaMKCreERT2}^{\text{+/+}}$ ($\beta\text{-cat cKO}$) mice and LoxP littermates injected with tamoxifen at 1 m.

(B and C) Spine pruning (B, n = 27–40/group) and maturation (C) were impaired in $\beta\text{-cat cKO}$ mice.

(D and E) Representative examples of spines in S1BF of $\text{CamK2}\alpha\text{-Ncad(intra)}$ mice and wild-type (WT) littermates (D), as well as cdf/cdf mice and control littermates (E).

(F and G) Spine pruning (F, n = 30–50/group) and maturation (G, 3 m) were impaired in $\text{CamK2}\alpha\text{-Ncad(intra)}$ mice.

(H and I) 3 m cdf/cdf mice showed higher spine density (H, n = 25–30/group) and less mature spines (I).

Scale bars, 5 μm . Data are presented as mean \pm SEM. See also Figure S2.

requirement of β -catenin during experience-dependent spine pruning. Similar pruning and maturation defects were also found in the $\text{CamK2}\alpha\text{-Ncad(intra)}$ transgenic mice (Figures 2D, 2F, and 2G), in which overexpression of the intracellular domain of N-cadherin sequestered endogenous β -catenin and interfered with normal functioning of the complex (Yu and Malenka, 2003). In homozygous cerebellar deficient folia (cdf) mice, in which the Catna2 gene encoding $\alpha\text{-N}$ -catenin is deleted, spine density was normal at 1 and 2 m, but significantly higher at 3 m, accompanied by significant reduction in the proportion of mature spines (Figures 2E, 2H, 2I, S2H, and S2I). Thus, in three independent genetic manipulations interfering with the function of the cadherin/catenin complex, we observed concurrent defects in spine pruning and maturation, implicating an important role of this complex in mediating these processes.

Locally Enhancing Cadherin/Catenin-Dependent Adhesion Induces β -Catenin Redistribution and Spine Fate Differentiation In Vitro

Having shown that β -catenin is required for spine pruning and maturation, we next asked if local changes in cadherin/cat-

enin-dependent adhesion were sufficient to induce the process. To track activity- or β -catenin-dependent changes at the single spine level, cultured neurons were co-transfected with GFP- β -catenin and tdTomato and imaged every hour upon local induction of cadherin-dependent adhesion using N-cad-Fc-coated beads. Using a paired spines analysis (PSA) (see Experimental Procedures), we compared spine pairs on the same dendritic branch, one in close contact with a N-cad-Fc bead (bead+ spine) and a neighboring spine not contacted by beads (bead- spine). During a 4-hr imaging period, we found that both GFP- β -cat intensity and spine size gradually increased in bead+ spines and were concurrently reduced in neighboring bead- spines, sometimes disappearing all together (Figures 3A, 3B, 3D, and 3E). As control, we showed that coating beads with human Fc did not significantly affect GFP- β -cat distribution or spine size (Figures 3C, 3F, and 3G). The likelihood of the bead- spine disappearing was not related to initial spine size (Figure 3H).

Consistent with the GFP- β -cat result, N-cad-Fc bead applications enriched surface N-cadherin, indicated by increased pHluorin-N-cadherin (pH-N-cad) intensity in the bead+ spines

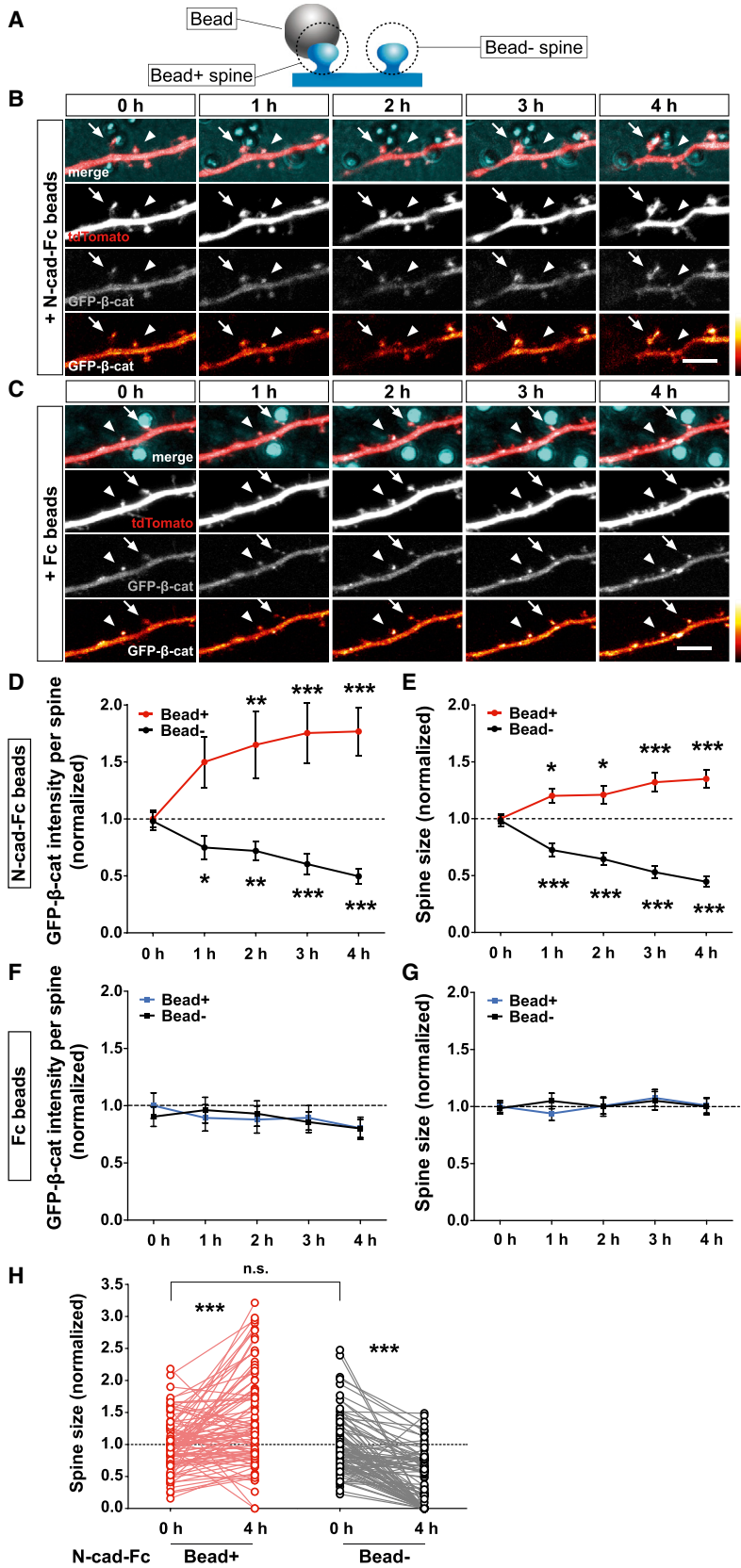


Figure 3. Locally Enhancing Cadherin/Catenin-Dependent Adhesion Differentiates Spine Fates In Vitro

(A) Schematic showing bead-contacting (bead+) and non-contacting (bead-) spines selected for PSA.

(B and C) Time-lapse images showing spine pairs expressing GFP- β -cat in contact with N-cad-Fc beads (B) or Fc control beads (C, bead+, arrow; bead-, arrowhead). Last row of each image set is in glow scale.

(D and E) PSA results showing changes in GFP- β -cat intensity (D) and spine size (E) between spine pairs in contact with N-cad-Fc beads ($n = 90$; bead+ versus bead-: D, 0 hr, n.s., 1 hr, $p < 0.01$, all others, $p < 0.001$; E, 0 hr, n.s., all others, $p < 0.001$).

(F and G) PSA results showing changes in GFP- β -cat intensity (F) and spine size (G) between spine pairs in contact with Fc beads ($n = 82$; bead+ versus bead-: n.s. for all time points).

(H) Plots of the size of 90 spine pairs analyzed in (D) and (E) before and after 4 hr-contact with N-cad-Fc beads. Paired t test, bead+ versus bead- at 0 hr, $p = 0.69$.

Scale bars, 5 μ m. Data are presented as mean \pm SEM.

and concurrent loss of pH-N-cad signal and reduced size of neighboring bead–spines (Figures 4A–4C). When all spine pairs were sorted into groups according to their survival status (both present, bead+ present only, bead– present only, both disappeared, Figure 4D), it was clear that contact with N-cad-Fc beads significantly enhanced the survival of bead+ spines, while simultaneously reducing that of neighboring bead– spines (Figures 4D and 4E).

Is the ability to induce spine fate differentiation specific to the cadherin/catenin complex? We thus tested a pair of heterophilic cell adhesion molecules well-known for their synaptogenesis functions, namely Neuroligin (NL) and Neurexin (NRXN) (Giagtzoglou et al., 2009; Südhof, 2008). Consistent with their synaptogenic abilities, spines contacting NRXN-1β-Fc-coated beads accumulated NL1-GFP and grew in size. However, the neighboring bead–spine did not shrink and even started to accumulate small amounts of NL1-GFP (Figures 4F–4H). Thus, the ability to simultaneously induce enlargement of one spine and pruning of its neighbor is specific to the cadherin/catenin complex. Further fluorescence recovery after photobleaching (FRAP) experiments showed that N-cadherin traveled in and out of spines faster than NL1 or the AMPA receptor subunit GluA2, as suggested by a shorter recovery half-time, a smaller time constant τ , and a larger rate constant K (Figures S3A–S3F), though NL1 had a larger mobile fraction (Figure S3G). Interestingly, the recovery curve of GluA2 fluorescence, similar to a previous report (Ashby et al., 2006), closely resembled that of N-cadherin, consistent with the reported physical interaction between GluA2 and N-cadherin (Saglietti et al., 2007).

Activity Induces Distance-Dependent Spine Fate Differentiation In Vitro

Are local differences in activity sufficient to induce redistribution of the cadherin/catenin complex and changes in spine fate? To address this question, we electroporated teal fluorescent protein (TFP)-tagged channelrhodopsin (ChR) into 10%–30% of neurons at time of plating and then co-transfected Venus-β-cat and tdTomato into another neuronal population (<1%) at 9 days in vitro (DIV), thereby allowing identification of juxtaposed pre-synaptic ChR axons and post-synaptic Venus-β-cat/tdTomato spines (Figure S4A). During live imaging at DIV 16, neurons were stimulated with blue light at 4 Hz (10 pulses of 10 ms, every 60 s), in the presence of tetrodotoxin to prevent recurrent activity. PSA was carried out between spine pairs, comparing a spine contacted by ChR axons (ChR⁺ spines, Figures 5A and 5C) with a neighboring spine not in contact with any ChR axons (ChR⁻ spines). We found that photostimulation induced enlargement of ChR⁺ spines, as well as their accumulation of Venus-β-cat. Importantly, neighboring ChR⁻ spines lost Venus-β-cat and shrank in size, sometimes disappearing all together (Figures 5A, 5D, and 5E; TFP Ctrl: Figures S4B and S4C).

To better quantitate these changes, we calculated a competition index (CI) (see Experimental Procedures) between ChR⁺ and ChR⁻ spines, with a CI toward “1” indicating that the ChR⁺ spine is winning, toward “−1” indicating that the ChR⁻ spine is winning, and a CI of “0” indicating no differences between ChR⁺ and ChR⁻ spines (Figure 5F). Use this simplified parameter, we found that activity-induced increase in CI was inversely corre-

lated with inter-spine distance (Figures 5G, S4G, and S4H) and independent of the number of in between spines (Figure S4I), further supporting a model of local competition for limited resources.

Activity-Induced Spine Fate Differentiation Requires Cadherin/Catenin-Dependent Adhesion but Not Protein Synthesis or Degradation

To further examine requirement for the cadherin/catenin complex in activity-induced spine fate differentiation, we imaged spines in neurons expressing GFP and in contact with ChR-tdTomato axons, with or without β-catenin RNAi. We found that photostimulation-induced spine fate differentiation was abolished in neurons with reduced endogenous β-catenin, (Figures 5B, 5H, and S4E). This effect was fully rescued by co-expression of Ncad-AD (Figures 5H and S4F), a chimera molecule consisting of the extracellular and transmembrane domain of N-cadherin fused with the actin-binding domain of αN-catenin and capable of restoring function of the cadherin/catenin complex in the absence of β-catenin (Tan et al., 2010). Together, these results demonstrate that β-catenin, specifically through its function as a component of the cadherin/catenin complex, is required for activity-induced spine fate differentiation.

Consistently, we showed in cross cell comparisons in fixed neuronal cultures that redistribution of β-catenin and differentiation of spine fate still occurred in the presence of the protein synthesis inhibitor cycloheximide (CHX) (Figures S5A and S5C). Interfering with proteasome-dependent protein degradation using MG132 or lactacystin (Lacta) also did not block either process, while application of tetanus toxin (TeTx) (Figures S5A and S5C) to inhibit synaptic transmission did. Importantly, interfering with N-cadherin surface mobility by crosslinking surface N-cadherin with an antibody against its surface epitope (N-cad Ab cross) or using N-cad-Fc-coated beads to sequester N-cadherin along dendritic shafts (N-cad-Fc sequester) (Figures S5A–S5D) effectively blocked both processes. The requirement of actin reorganization and Ca²⁺/calmodulin-dependent protein kinase II (CaMKII) activity, but not protein synthesis, for coordinated spine fate differentiation and β-catenin redistribution was further confirmed by live imaging within the first hour of photostimulation (Figures S5E–S5L). Together, these results strongly suggest a critical role of inter-spine competition for the cadherin/catenin complex in local, activity-induced differentiation of spine fates.

Inter-Spine Competition for β-Catenin Biases Spine Fate In Vivo

Does inter-spine competition for β-catenin also mediate spine pruning in vivo? To investigate this, we injected AAV-Cre-GFP into the S1BF of 1-month-old Ai34D; β-cat^{Δex3/Δex3} mice, where Cre expression (Cre⁺) induced expression of a truncated and stabilized form of β-catenin (β-cat Ovp) (Harada et al., 1999) (Figures 6A, S6A, and S6B), as well as synaptophysin-tdTomato (Ai34D) to mark presynaptic axonal termini (pre. β-cat Ovp, Figures 6A, 6C, and 6D); Ai34D mice injected with AAV-Cre-GFP were used as controls (pre. Ctrl, Figures 6A, 6C, and 6D). Two weeks after viral injection, uninfected layer 2/3 pyramidal neurons near the injection site were filled with the green

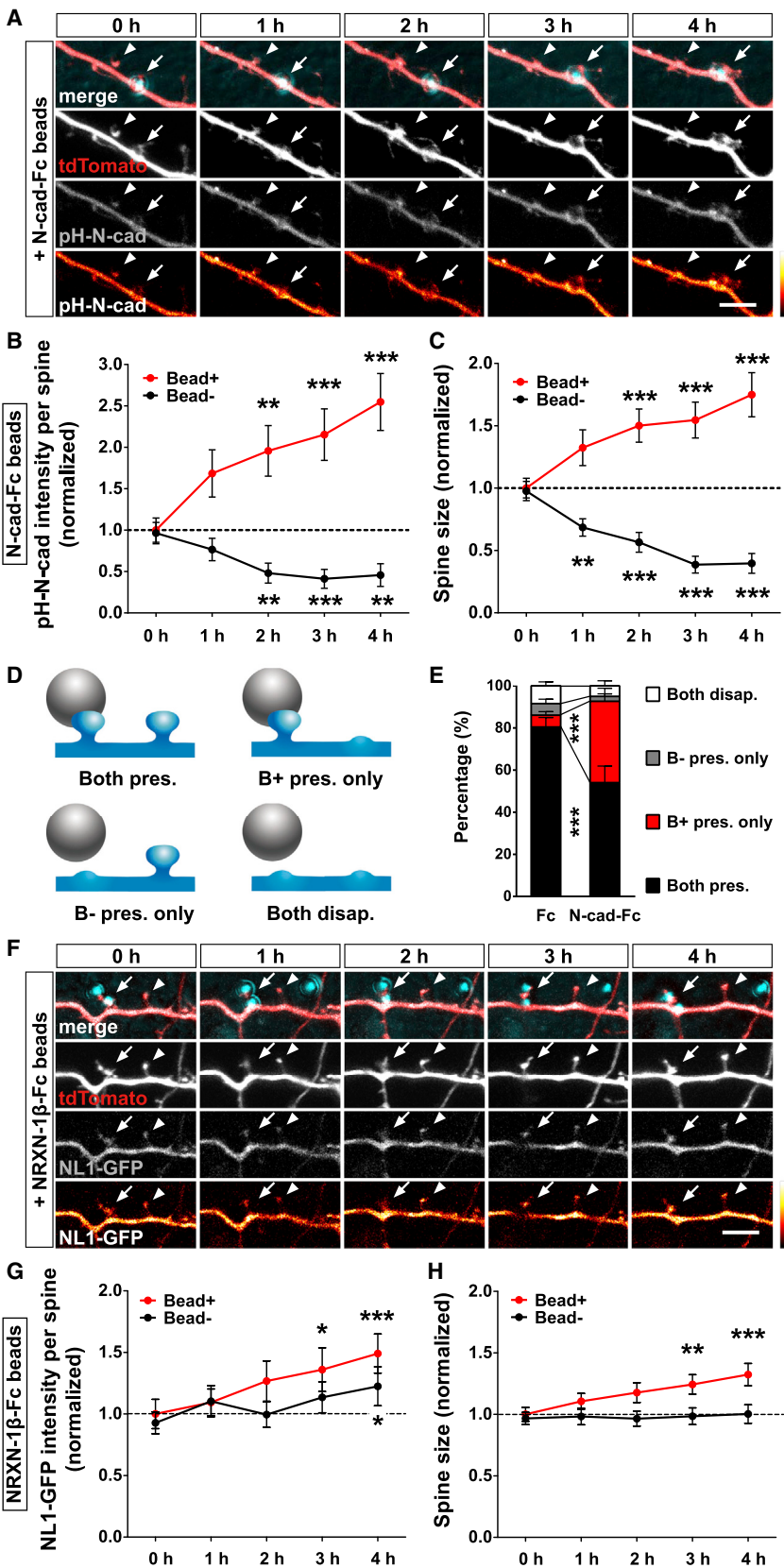


Figure 4. The Ability to Induce Spine Fate Differentiation Is Specific to the Cadherin/Catenin Complex

(A and F) Time-lapse images showing spine pairs expressing pH-N-cad in contact with N-cad-Fc beads (A) or spines expressing NL1-GFP in contact with NRXN-1 β -Fc beads (F, bead+, arrow; bead-, arrow-head), last row in glow scale.

(B and C) PSA results showing changes in pH-N-cad intensity (B) and spine size (C) between spine pairs in contact with N-cad-Fc beads ($n = 41$; bead+ versus bead-: B, 0 hr, n.s., 1 hr, $p < 0.05$, all others, $p < 0.001$; C, 0 hr, n.s. all others, $p < 0.001$).

(D and E) Schematics (D) and distributions (E) of 4 types of spine pairs at the end of imaging ($n = 7$ experiments in Fc, 9 in N-cad-Fc).

(G and H) PSA results showing changes in NL1-GFP intensity (G) and spine size (H) between spine pairs in contact with NRXN-1 β -Fc beads ($n = 81$; bead+ versus bead-: G, n.s. for all time points; H, 0–2 hr, n.s., 3 hr, $p < 0.05$, 4 hr, $p < 0.01$).

Scale bars, 5 μ m. Data are presented as mean \pm SEM. See also Figure S3.

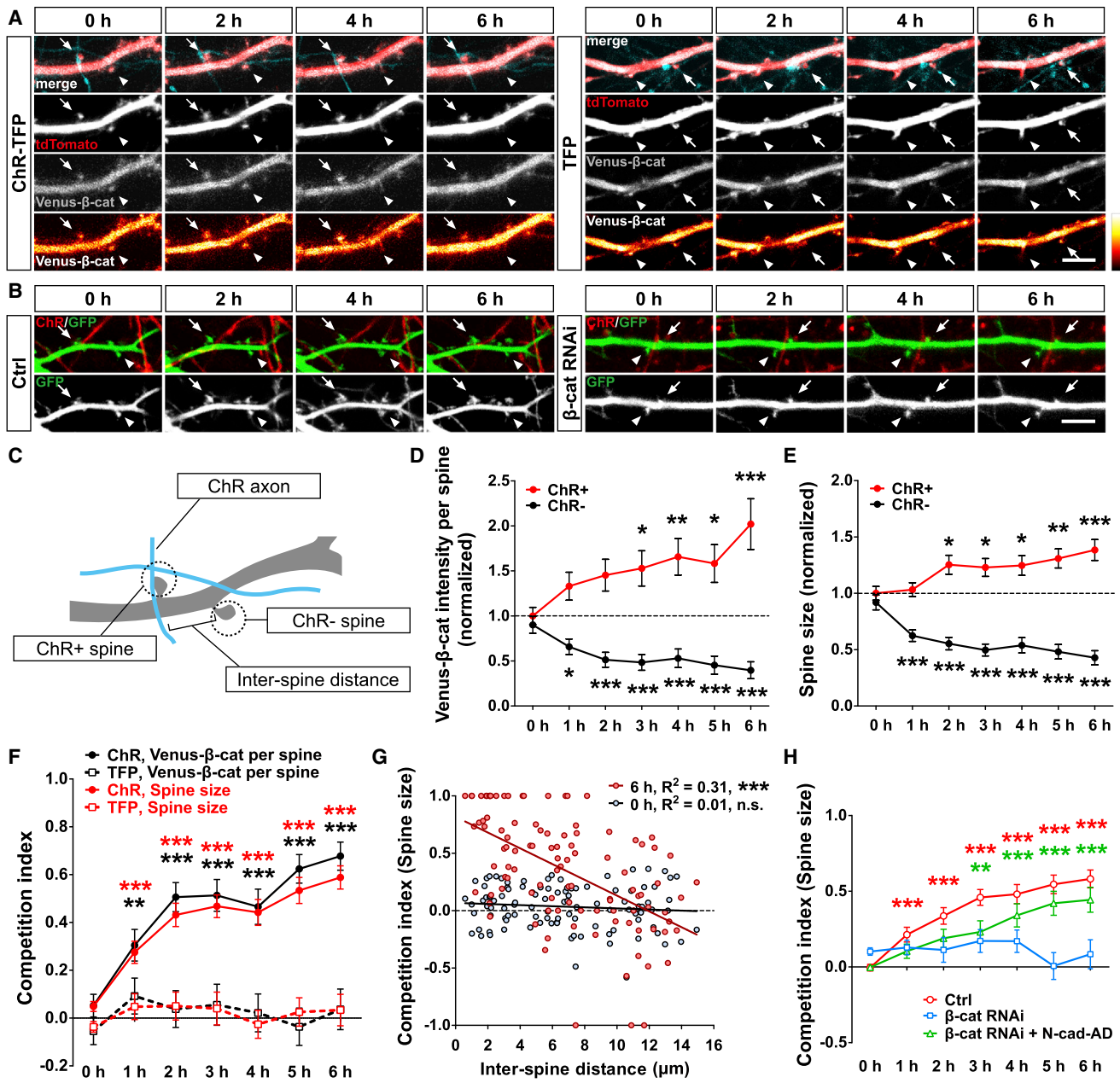


Figure 5. Activity Induces In Vitro Spine Fate Differentiation Mediated by β-Catenin

(A and B) Time-lapse images showing spine pairs (A, red; B, green) contacting ChR-TFP (A, cyan) or ChR-tdTomato (B, red) axons (ChR+, arrow; ChR-, arrowhead).

(C) Schematics of ChR^{+/−} spine pairs selected for PSA.

(D–F) PSA results showing changes in Venus-β-cat intensity (D), spine size (E), and competition indices (Cl, F) between the paired spines ($n = 58\text{--}64$, ChR⁺ versus ChR[−]: D, 0 hr, n.s., 1 hr, $p < 0.05$, all others, $p < 0.001$; E, 0 hr, n.s., 1 hr, $p < 0.01$, all others, $p < 0.001$).

(G) An inverse correlation between Cls (spine size) and inter-spine distances at 6 hr ($n = 105$).

(H) The increase of Cl in ChR spine pairs (red, $n = 56$) was abolished by β-catenin RNAi (blue, $n = 23$), and restored by co-expression of N-cad-AD (green, $n = 34$). Scale bars, 5 μm. Data are presented as mean ± SEM. See also Figures S4 and S5.

fluorescent dye Alexa 488 to visualize their spine morphology. PSA was carried out for green spines contacting pre-synaptic Ai34D puncta (Ai⁺ spines) via recurrent layer 2/3 connections and adjacent spines on the same dendrite not contacting

Ai34D puncta (Ai[−] spines). In control Ai34D mice, all neurons are genetically wild-type for β-catenin, both pre- and post-synaptically, and no differences were observed in the relative sizes of Ai⁺ and Ai[−] spines (Figures 6D and 6E; Movie S1). In

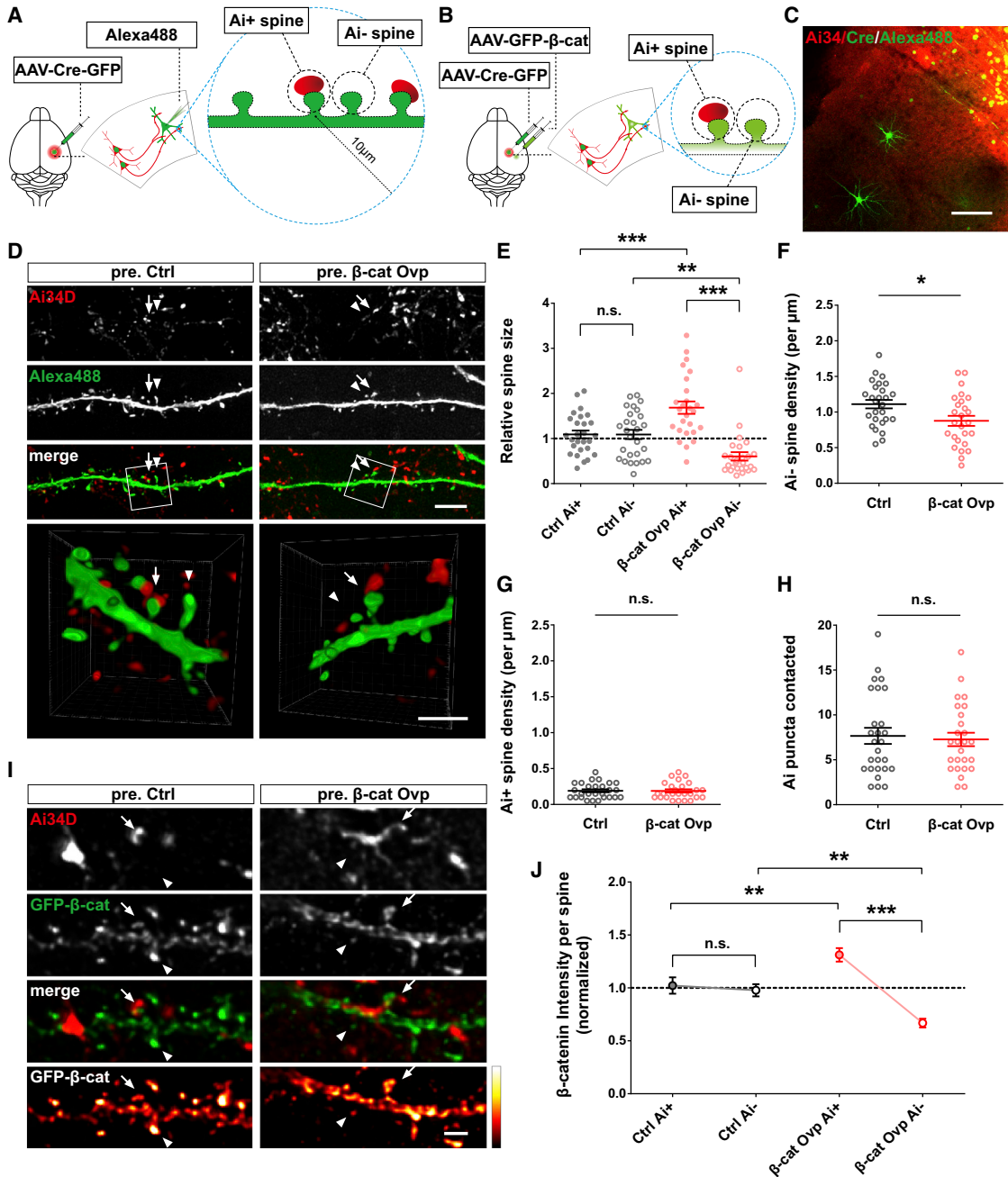


Figure 6. Inter-Spine Competition for β -Catenin Differentiates Spine Fates In Vivo

(A and B) Schematics of viral injection and dye microinjection experiments in floxed Ai34D; β -cat $^{\Delta\text{ex3}/\Delta\text{ex3}}$ mice or Ai34D mice for in vivo PSA of spine size (A) and β -catenin level (B).

(C) Merged image showing Cre-GFP (green nuclear fluorescence, upper right corner), Ai34D (red), and Alexa 488 dye-fill (green neurons with clear morphology, bottom left).

(D) Representative deconvolved images showing spine pairs (green) contacting Ai34D (red) puncta (Ai⁺, arrow; Ai⁻, arrowhead) in Ctrl (pre. Ctrl) and presynaptic β -catenin overexpressing (pre. β -cat Ovp) mice. The magnified and 3D-rendered views of spines in the boxed region (white box in third row) are shown in the bottom row.

(E) PSA results showing changes in relative spine size between spine pairs ($n = 26-27$). Dotted line indicates the average size of all spines within 10 μm radius of the Ai⁺ spine.

(F-H) The densities of Ai⁻ (F) and Ai⁺ spines (G), as well as the number of Ai34D puncta contacted by filled dendrite/spines (H) within 10 μm radius of the Ai⁺ spine.

(I) Representative deconvolved images showing spine pairs expressing GFP- β -cat (green) and contacting Ai34D (red) puncta (Ai⁺, arrow; Ai⁻, arrowhead) in pre. Ctrl and pre. β -cat Ovp mice.

(legend continued on next page)

Ai34D; $\beta\text{-cat}^{\Delta\text{ex3}/\Delta\text{ex3}}$ mice, the post-synaptic filled neurons did not express Cre and thus had wild-type β -catenin level, while pre-synaptic Ai34D puncta contacting Ai^+ spines had higher levels of presynaptic β -catenin and thus could recruit more cadherin/catenin complexes into the contracting spine. In other words, presynaptic $\beta\text{-cat}$ Ovp by Cre expression in Ai34D; $\beta\text{-cat}^{\Delta\text{ex3}/\Delta\text{ex3}}$ mice achieved the *in vivo* equivalent of the N-cad-Fc beads (Figures 3 and 4). PSA showed that Ai^+ spines in pre. $\beta\text{-cat}$ Ovp mice were larger in size than neighboring Ai^- spines and both also respectively larger and smaller than their counterparts in pre. Ctrl mice (Figures 6D and 6E; Movie S2). We also found that within a 10 μm radius of each Ai^+ spine, the density of Ai^- spines was significantly lower in pre. $\beta\text{-cat}$ Ovp mice, as compared with pre. Ctrl mice (Figure 6F), while no significant changes were found in Ai^+ spine density (Figure 6G). This reduction in Ai^- spine density was not induced by alterations in the probability of spines contacting Ai34D puncta, since the total number of Ai puncta in contact with the dendritic segment was not significantly different between Ctrl and $\beta\text{-cat}$ Ovp mice (Figure 6H). Together, these results suggest that enhancing cadherin/catenin-dependent adhesion on an individual spine *in vivo* was sufficient to make it more mature and at the same time destabilizes and/or eliminates neighboring spines.

In a complementary set of experiments, we injected AAV-Cre-GFP and AAV-GFP- β -cat (Figure S6C) into two different but close sites in the S1BF of Ai34D; $\beta\text{-cat}^{\Delta\text{ex3}/\Delta\text{ex3}}$ mice. Neurons infected with the two constructs were highly distinguishable: those expressing Cre showing strong nuclear Cre-GFP signals, as well as Ai34 puncta at their axonal termini, while those expressing GFP- β -cat had GFP-tagged β -catenin in their dendrites and spines (Figures 6B and 6I). PSA results showed that in Ctrl mice, 2 weeks after viral injection, GFP- β -cat was equally distributed between Ai^+ and Ai^- spines (Figures 6I and 6J). However, in pre. $\beta\text{-cat}$ Ovp mice, the Ai^+ spines possessed a higher level of GFP- β -cat while neighboring Ai^- spines generally lost GFP- β -cat (Figures 6I and 6J). Together these results demonstrate that differential levels of cadherin/catenin-dependent adhesion between neighboring spines are sufficient to induce *in vivo* redistribution of β -catenin between spines and direct them into the distinct fates of becoming more mature or being eliminated.

In the experiments above, differences between spines within the same neuron were induced. There is an alternative scenario where local differences in post-synaptic β -catenin level between spines of different neurons could bias their competition for a common pre-synaptic axonal terminus (Holtmaat and Svoboda, 2009; Knott et al., 2006; Lee et al., 2013). Deducing from our inter-spine competition model, we would expect that between such neighboring neurons, the one with higher total β -catenin level would be advantaged and thus have a higher spine density. We induced differential β -catenin expression between neighboring neurons by sparsely infecting S1BF in one cerebral hemisphere of $\beta\text{-cat}^{fl/fl}$ mice ($\beta\text{-cat}$ cKO) with AAV-Cre-GFP (~30% of

all glutamatergic neurons infected) at 1 m and the other hemisphere with AAV-GFP as control (Figure S6D). At 2 or 3 m, three types of neurons were analyzed: Cre⁺ neurons with reduced β -catenin level, Cre⁻ neurons within 50 μm radius of Cre⁺ neurons (wild-type β -catenin level), and GFP control neurons from the other hemisphere (wild-type β -catenin level). At both ages, Cre⁺ neurons had lower spine density and at 3 m also a lower proportion of mature spines as compared with neighboring Cre⁻ neurons or control GFP neurons (Figures S6E and S6G–S6J). These results support the notion that intracellular β -catenin provided “competence” for spine survival and maturation.

When similar experiments were performed in $\beta\text{-cat}^{\Delta\text{ex3}/\Delta\text{ex3}}$ mice, $\beta\text{-cat}$ Ovp Cre⁺ neurons had a higher spine density and accelerated spine maturation (Figures S6F and S6K–S6N). Importantly, Cre⁻ neurons neighboring Cre⁺ $\beta\text{-cat}$ Ovp neurons had significantly lower spine density and less mature spines as compared with GFP neurons, even though they genetically both have wild-type β -catenin levels (Figures S6F and S6K–S6N). Thus, the fates of individual spines depend not only on their own β -catenin level, but also on their relative level with neighboring “competitor” spines sharing similar axonal inputs.

Acceleration of Spine Pruning by Enrichment Requires β -Catenin

To examine if the cadherin/catenin complex was required for enrichment-induced acceleration of spine pruning, we densely infected S1BF of 1-month-old $\beta\text{-cat}^{fl/fl}$ mice reared under control or EE conditions with AAV-Cre-GFP (~90% glutamatergic neurons infected) and with AAV-GFP in the opposite hemisphere as a control. Consistent with our Golgi staining data (Figures 1A–1C and 2A–2C), EE yielded significant acceleration of spine pruning and maturation in LoxP control neurons, while both processes were significantly blocked in $\beta\text{-cat}$ cKO neurons (Figures 7A–7D; neurons with severe dendrite blebbing, termed Type II neurons, were excluded from analyses, see Figures S7A–S7D). In EE-reared mice, although $\beta\text{-cat}$ cKO neurons still underwent some level of pruning, their spine densities at 2 and 3 m were significantly higher than those of LoxP control neurons and similar to that of $\beta\text{-cat}$ cKO neurons in Ctrl mice (Figures 7A and 7B). More importantly, spine maturation was completely blocked in $\beta\text{-cat}$ cKO neurons under EE conditions (Figure 7D). These results demonstrated that experience-induced acceleration of spine pruning and maturation required β -catenin function, although enrichment may partially compensate the pruning defects in $\beta\text{-cat}$ cKO neurons, probably through activation of alternative mechanisms. In support of the limited resource hypothesis, enrichment did not significantly affect N-cadherin and β -catenin levels (Figures S7E–S7G).

DISCUSSION

The neural circuitry in the mammalian brain undergoes substantial remodeling during postnatal development. Here we

(J) PSA results showing GFP- β -cat level in spine pairs ($n = 76$ –102). Dotted line indicates the average GFP- β -cat intensity of all spines measured along the same dendrite.

Scale bars, 100 μm in (C), 5 μm in third row of (D), 2 μm in the bottom row of (D) and in (I).

Data are presented as mean \pm SEM. See also Figure S6 and Movies S1 and S2.

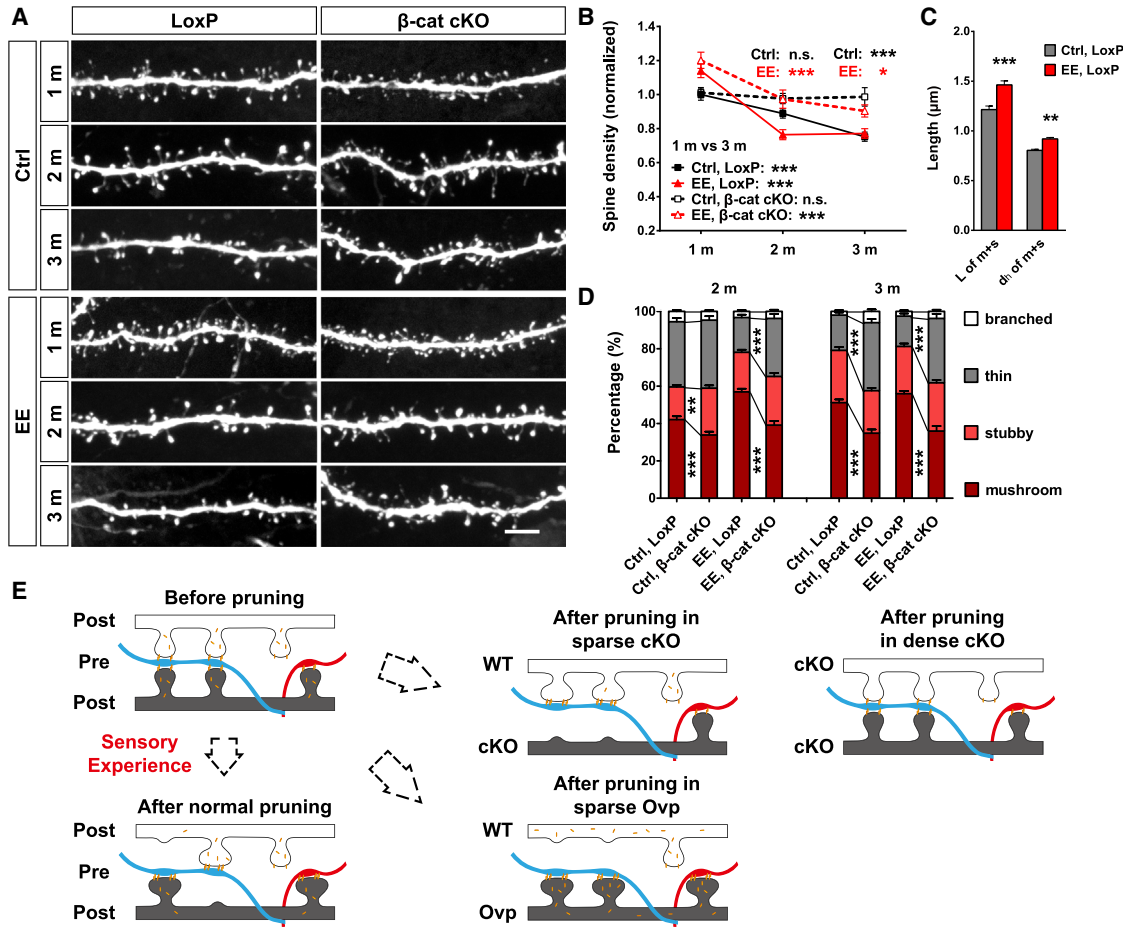


Figure 7. Reduction in Endogenous β -Catenin Level Prevents Enrichment-Induced Acceleration of Spine Pruning and Maturation

(A) Representative images of spines of neurons in β -cat^{fl/fl} mice infected with AAV-GFP (LoxP) or AAV-Cre-GFP (β -cat cKO) at 1 m.

(B–D) Spine pruning (B, n = 24–38/group) and maturation (D) in β -cat cKO neurons were both impaired under Ctrl and EE conditions. The length and head diameter of mushroom and stubby spines in LoxP neurons are shown in (C; n = 200/group).

(E) A competition-based model of spine pruning.

Scale bars, 5 μm . Data are presented as mean \pm SEM. See also Figure S7.

demonstrated that during brain maturation, neural activity drives neighboring spines to compete for limited cadherin/catenin complexes, resulting in redistribution of cadherins and catenins from less active spines to the more active spines, leading to concurrent maturation of the latter and elimination/pruning of the former. This activity-driven, cadherin/catenin-dependent and competition-based model for coordinated spine pruning and maturation (Figure 7E) provides a molecular mechanism for specificity during neural circuit refinement. In light of previous work showing regulation of spine density via competition between neurons for limited resources (English et al., 2012; Kwon et al., 2012), this work demonstrates that the competition can occur at the more subcellular level of neighboring spines on the same dendritic branch. Thus, it may represent a basic principle in neuroscience that limited availability of specific molecules determines the normal wiring of the brain and defect of which may result in neuropsychiatric disorders.

Activity-Dependent Spine Pruning in Multiple Brain Regions

Spine pruning is a well-characterized phenomenon that occurs across mammalian species (Alvarez and Sabatini, 2007; Bhattacharyya et al., 2009; Fu and Zuo, 2011; Holtmaat and Svoboda, 2009). Here, we demonstrate that spine pruning occurs at the population level in multiple sensory-motor regions of the rodent brain, as well as medium spiny neurons of the dorsal striatum (Figures 1 and S1A–S1D). While the causal relationship between spine dynamics and memory remains to be demonstrated conclusively (Hübener and Bonhoeffer, 2010), the observations that sensory experience, motor learning, and fear conditioning all affected the rates of both spine formation and elimination (Fu et al., 2012; Holtmaat et al., 2006; Lai et al., 2012; Trachtenberg et al., 2002; Xu et al., 2009; Yang et al., 2009; Zuo et al., 2005b), clearly demonstrate a strong correlation between spine dynamics and experience-dependent learning. We surmise that in the sensory/motor cortices, spine pruning occurs at the

population level, likely because development within each region is relatively synchronized in order to learn “routines,” such as differentiating shapes, textures, and odors and acquiring motor skills like walking, climbing, and whisking, abilities that remain relatively constant throughout adulthood.

In the PFC and hippocampus, in contrast, new memories are constantly formed and unconsolidated ones removed throughout life, a few synapses at a time, resulting in individualized spine dynamics and sustained circuit plasticity. In our experiments, the most significant effect of EE in these regions was slightly increased spine density at one development time point (Figures S1E and S1F), possibly generating more potential for plasticity in adulthood. This result is in contrast to the population level spine pruning observed in the PFC of post-mortem human and non-human primates. Interestingly, both spinogenesis and spine pruning are delayed in the PFC, as compared to sensory cortices, in humans (Huttenlocher, 2002), while in non-human primates, spinogenesis was similar between different regions, but spine pruning was more protracted in the PFC (Elston et al., 2009; Rakic et al., 1986, 1994). This evolutionary change in PFC spine dynamics likely reflects the increasing importance of the PFC for higher cognitive tasks in primates and especially humans.

Cadherin/Catenin-Dependent and Competition-Based Model for Coordinated Spine Pruning and Maturation

The molecular mechanism by which spines are selectively pruned during brain maturation has been a long-standing mystery. Here, we demonstrate that spine pruning is highly coordinated with spine maturation and is an inevitable consequence of activity-induced inter-spine competition for limited intracellular resource, which we identified to be the cadherin/catenin complex (Figure 7E).

The cadherin/catenin complex is synaptically localized and has well-described roles in promoting spinogenesis (Arikkath and Reichardt, 2008; Benson and Huntley, 2012; Brigidi and Bamji, 2011; Tai et al., 2008). Here, we demonstrate that local redistribution of β -catenin via inter-spine competition is necessary and sufficient for mediating spine pruning (Figures 3, 4, 5, 6, and S6). The dependence of this process on inter-spine distance (Figure 5G) and N-cadherin motility (Figures S5A–S5D), but not on protein synthesis or degradation (Figures S5A, S5C, S5H, and S5L), strongly suggests that competition for surface cadherin/catenin complexes is the main driving force underlying initial spine fate determination. Consistently, activity has been previously shown to locally regulate N-cadherin endocytosis (Tai et al., 2007), an important step for relocating cadherin/catenin complexes between spines, and stabilize trans-synaptic cadherin/catenin complexes (Tanaka et al., 2000). The competition-based model of spine pruning is further supported by our *in vivo* observations that under all conditions where neighboring neurons had similar β -catenin levels (Figures 1, 2, and 7), as would occur naturally, spine pruning and maturation are always coordinated, demonstrating tight coordination between these processes *in vivo*.

Is the role of cadherin/catenin complex in mediating coordinated spine maturation and pruning related to its spinogenesis effects? We believe these to be distinct functions. In its syn-

aptogenesis function, loss of β -catenin at the population level reduced spine density (Arikkath and Reichardt, 2008; Benson and Huntley, 2012; Brigidi and Bamji, 2011; Tai et al., 2008). In contrast, in the concurrent spine maturation and pruning function we identify here, β -catenin loss at the population level resulted in pruning defects and higher overall spine density (Figures 2A–2C and 7A–7D). The behavior of the cadherins/catenins is distinct from that of the NLs/NRXNs, another well-studied pair of cell adhesion molecules known for their strong synaptogenic effects (Giagtzoglou et al., 2009; Südhof, 2008). Locally clustering NLs induced spine enlargement, without inducing pruning of its neighbors (Figures 4F–4H). This important difference distinguishes NL from N-cadherin, with the former being strictly synaptogenic, and the latter having a weaker synaptogenic role, but later on playing important roles in the refinement of neural circuitry. We note that N-cadherin is homophilic, which may facilitate coordinated pre- and post-synaptic interactions, as only the expression of one molecule needs to be regulated.

Abnormal Spine Pruning in Neurodevelopmental Disorders

Loss- and gain-of-function of a number of molecules have already been shown to both result in neurological disorders with developmental origins, including ASD, intellectual disability, and schizophrenia (Glausier and Lewis, 2013; Penzes et al., 2011; Zoghbi and Bear, 2012), underscoring the importance of appropriate gene expression for normal neural circuit development. N-cadherin and β -catenin, by virtue of their early expression in embryonic development, are essential for survival of the embryo and thus not genetically associated with neuropsychiatric disorders. However, other catenins with overlapping functions, including *Ctnna2* and *Ctnnd2*, as well as classical cadherin family members with more restricted expression patterns, such as *Cdh7*, *Cdh9*, *Cdh10*, *Cdh12*, *Cdh15*, and *Cdh18*, have been linked to ASD, intellectual disability, bipolar disorder, and schizophrenia (Hirano and Takeichi, 2012; Redies et al., 2012; Turner et al., 2015).

Increased spine density has been observed in adolescent postmodern autism patients but not younger ones, suggesting defects in spine pruning in ASD patients. In contrast to schizophrenia, where spine density abnormalities were restricted to the PFC (Glausier and Lewis, 2013), spine pruning defects in ASD patients were found in all brain areas examined, including temporal, parietal, and frontal regions (Hutsler and Zhang, 2010; Tang et al., 2014). Abnormalities in spine pruning have also been reported in multiple sensory regions in ASD mouse models such as *Fmr1* KO and *MECP2* duplication (He and Portera-Cailliau, 2013; Penzes et al., 2011; Zoghbi and Bear, 2012). Since “hypersensitivity and hyposensitivity to sensory inputs” is prevalent among children with ASD (Marco et al., 2011; Suarez, 2012), defects in spine pruning in sensory cortices could be a contributing factor to the observed changes in sensory inputs. Furthermore, given the fundamental roles of dendritic spines in shaping neural circuitry and neural plasticity, the regulation of spine pruning by cadherin/catenin complexes, in the context of existing literature, may provide the missing link through which alterations in transcription factors such as

FMRP and MeCP2 can lead to autism, intellectual disability, and related neurodevelopmental disorders.

EXPERIMENTAL PROCEDURES

Full experimental details can be found in the [Supplemental Experimental Procedures](#).

Viral Injections, Immunohistochemistry, and Fluorescent Dye Microinjections

All animal procedures complied with the animal care standards set forth by the US NIH and have been approved by the Institutional Animal Care and Use Committee of the Institute of Neuroscience, Chinese Academy of Science (Shanghai, China). Mice injected with adeno-associated viruses (AAVs, packaged by Obio Technology) were perfused with PBS, followed by 4% paraformaldehyde. Coronal sections (30 μm) were used for immunohistochemistry and 250 μm sections for dye microinjections, carried out on a Nikon FN1 fluorescence microscope using sharp glass pipettes loaded with fluorescent dyes.

Image Acquisition and Live Imaging

For *in vivo* spine analysis, basal dendrites of layer 2/3 pyramidal neurons were imaged at 1 μm (Golgi staining) or 0.3 μm (dye microinjection) Z intervals.

Live imaging experiments were performed using DIV16 neurons. For beads experiments, protein-coated beads were applied to the cultures 30 min before imaging to allow the beads to sink to the bottom of the dish. For photostimulation, a custom-made LED system controlled by Master-8 (A.M.P.I.) was used to deliver a train of blue light pulses every 60 s.

Image Analyses

All images were analyzed with no post-acquisition modifications and blinded to the experimental condition. PSA was performed in ImageProPlus by randomly selecting neighboring spines (regions of interest) on the same dendritic branch from images in the morphology marker channel and thresholded. A mask was then generated to measure spine area and total intensity of fluorescently tagged proteins. The competition index (CI) was calculated as: $(pC^+ - pC^-)/(pC^+ + pC^-)$, in which “ p ” is the parameter of interest, i.e., spine size or integrated intensity of the labeled molecule and “ C^+ ” or “ C^- ” indicates whether the parameter was measured in a contacting (C^+) or non-contacting (C^-) spine, be it bead or ChR axon.

For *in vivo* comparison of Ai^+ and Ai^- spines, PSA was performed between Ai^+ spine and the nearest Ai^- spine on the same dendrite. A circle of radius 10 μm was drawn around the Ai^+ spine and the density of Ai^+ and Ai^- spine within that circle measured. The sizes of Ai^+/Ai^- spine pairs were normalized to the mean size of all spines in that circle, and GFP- β -cat intensity was normalized to the mean intensity of all spines analyzed on the same neuron (usually six to ten spines).

In example images, brightness/contrast adjustment within linear ranges were made using Fiji/ImageJ when necessary. Images in [Figures 6D](#) and [6I](#) and [Movies S1](#) and [S2](#) were deconvolved using Huygens Essential and 3D rendered in Imaris. For Golgi staining examples, images were projected at minimal intensity and inverted.

SUPPLEMENTAL INFORMATION

Supplemental Information includes Supplemental Experimental Procedures, seven figures, and two movies and can be found with this article online at <http://dx.doi.org/10.1016/j.cell.2015.07.018>.

AUTHOR CONTRIBUTIONS

W.-J.B. and X.Y. designed the project and wrote the manuscript. W.-J.B. performed all experiments and data analyses, except for western blots by W.-Y.M. and generation of molecular tools by S.-J.H. and Z.Q. All authors commented on the manuscript.

ACKNOWLEDGMENTS

We thank Drs. Klaus Nave, Makato M. Taketo, and the European Mutant Mouse Archive for transgenic mice, and Drs. Hailan Hu, Wei Lu, Thomas Sudhof, Chin-Yin Tai, Roger Tsien, and Yi-Zheng Wang for constructs. We thank He-Ling Song, Yuan Lu, Yue Sun, Zong-Fang Wan, Xue-Zhi Zeng, and Sha-Jin Huang for technical assistance and Dr. Yunqing Wen for help with the custom-made LED system. We thank the ION Optical Imaging Core Facility and Transgenic Core Facility for excellent technical support. We are grateful to colleagues at ION and members of the X.Y. laboratory for suggestions and comments. This work was supported by grants from the Ministry of Science and Technology (2011CBA00400) and the National Natural Science Foundation of China (31125015 and 31321091).

Received: October 29, 2014

Revised: April 11, 2015

Accepted: June 13, 2015

Published: August 6, 2015

REFERENCES

- Alvarez, V.A., and Sabatini, B.L. (2007). Anatomical and physiological plasticity of dendritic spines. *Annu. Rev. Neurosci.* **30**, 79–97.
- Arikkath, J., and Reichardt, L.F. (2008). Cadherins and catenins at synapses: roles in synaptogenesis and synaptic plasticity. *Trends Neurosci.* **31**, 487–494.
- Ashby, M.C., Maier, S.R., Nishimune, A., and Henley, J.M. (2006). Lateral diffusion drives constitutive exchange of AMPA receptors at dendritic spines and is regulated by spine morphology. *J. Neurosci.* **26**, 7046–7055.
- Benson, D.L., and Huntley, G.W. (2012). Synapse adhesion: a dynamic equilibrium conferring stability and flexibility. *Curr. Opin. Neurobiol.* **22**, 397–404.
- Bhatt, D.H., Zhang, S., and Gan, W.B. (2009). Dendritic spine dynamics. *Annu. Rev. Physiol.* **71**, 261–282.
- Bourne, J., and Harris, K.M. (2007). Do thin spines learn to be mushroom spines that remember? *Curr. Opin. Neurobiol.* **17**, 381–386.
- Bourne, J.N., and Harris, K.M. (2008). Balancing structure and function at hippocampal dendritic spines. *Annu. Rev. Neurosci.* **31**, 47–67.
- Brigidi, G.S., and Bamji, S.X. (2011). Cadherin-catenin adhesion complexes at the synapse. *Curr. Opin. Neurobiol.* **21**, 208–214.
- Cajal, S.R.y. (1911). *Histologie du Systeme Nerveux de l'Homme et des Vertébrés* (Maloine).
- Chen, J.L., Villa, K.L., Cha, J.W., So, P.T., Kubota, Y., and Nedivi, E. (2012). Clustered dynamics of inhibitory synapses and dendritic spines in the adult neocortex. *Neuron* **74**, 361–373.
- Elston, G.N., Oga, T., and Fujita, I. (2009). Spinogenesis and pruning scales across functional hierarchies. *J. Neurosci.* **29**, 3271–3275.
- Engert, F., and Bonhoeffer, T. (1999). Dendritic spine changes associated with hippocampal long-term synaptic plasticity. *Nature* **399**, 66–70.
- English, C.N., Vigers, A.J., and Jones, K.R. (2012). Genetic evidence that brain-derived neurotrophic factor mediates competitive interactions between individual cortical neurons. *Proc. Natl. Acad. Sci. USA* **109**, 19456–19461.
- Fu, M., and Zuo, Y. (2011). Experience-dependent structural plasticity in the cortex. *Trends Neurosci.* **34**, 177–187.
- Fu, M., Yu, X., Lu, J., and Zuo, Y. (2012). Repetitive motor learning induces coordinated formation of clustered dendritic spines *in vivo*. *Nature* **483**, 92–95.
- Giagtzoglou, N., Ly, C.V., and Bellen, H.J. (2009). Cell adhesion, the backbone of the synapse: “vertebrate” and “invertebrate” perspectives. *Cold Spring Harb. Perspect. Biol.* **1**, a003079.
- Glausier, J.R., and Lewis, D.A. (2013). Dendritic spine pathology in schizophrenia. *Neuroscience* **251**, 90–107.
- Govindarajan, A., Kelleher, R.J., and Tonegawa, S. (2006). A clustered plasticity model of long-term memory engrams. *Nat. Rev. Neurosci.* **7**, 575–583.
- Grutzendler, J., Kasthuri, N., and Gan, W.B. (2002). Long-term dendritic spine stability in the adult cortex. *Nature* **420**, 812–816.

- Harada, N., Tamai, Y., Ishikawa, T., Sauer, B., Takaku, K., Oshima, M., and Taketo, M.M. (1999). Intestinal polyposis in mice with a dominant stable mutation of the beta-catenin gene. *EMBO J.* 18, 5931–5942.
- Harris, K.M., and Weinberg, R.J. (2012). Ultrastructure of synapses in the mammalian brain. *Cold Spring Harb. Perspect. Biol.* 4, a005587.
- Harris, K.M., Jensen, F.E., and Tsao, B. (1992). Three-dimensional structure of dendritic spines and synapses in rat hippocampus (CA1) at postnatal day 15 and adult ages: implications for the maturation of synaptic physiology and long-term potentiation. *J. Neurosci.* 12, 2685–2705.
- He, C.X., and Portera-Cailliau, C. (2013). The trouble with spines in fragile X syndrome: density, maturity and plasticity. *Neuroscience* 251, 120–128.
- He, S., Ma, J., Liu, N., and Yu, X. (2010). Early enriched environment promotes neonatal GABAergic neurotransmission and accelerates synapse maturation. *J. Neurosci.* 30, 7910–7916.
- Hensch, T.K. (2004). Critical period regulation. *Annu. Rev. Neurosci.* 27, 549–579.
- Higley, M.J., and Sabatini, B.L. (2012). Calcium signaling in dendritic spines. *Cold Spring Harb. Perspect. Biol.* 4, a005686.
- Hirano, S., and Takeichi, M. (2012). Cadherins in brain morphogenesis and wiring. *Physiol. Rev.* 92, 597–634.
- Holtmaat, A., and Svoboda, K. (2009). Experience-dependent structural synaptic plasticity in the mammalian brain. *Nat. Rev. Neurosci.* 10, 647–658.
- Holtmaat, A.J., Trachtenberg, J.T., Wilbrecht, L., Shepherd, G.M., Zhang, X., Knott, G.W., and Svoboda, K. (2005). Transient and persistent dendritic spines in the neocortex *in vivo*. *Neuron* 45, 279–291.
- Holtmaat, A., Wilbrecht, L., Knott, G.W., Welker, E., and Svoboda, K. (2006). Experience-dependent and cell-type-specific spine growth in the neocortex. *Nature* 441, 979–983.
- Hübener, M., and Bonhoeffer, T. (2010). Searching for engrams. *Neuron* 67, 363–371.
- Huttsler, J.J., and Zhang, H. (2010). Increased dendritic spine densities on cortical projection neurons in autism spectrum disorders. *Brain Res.* 1309, 83–94.
- Huttenlocher, P.R. (2002). Neural Plasticity: the Effects of Environment on the Development of the Cerebral Cortex (Harvard University Press).
- Kasai, H., Matsuzaki, M., Noguchi, J., Yasumatsu, N., and Nakahara, H. (2003). Structure-stability-function relationships of dendritic spines. *Trends Neurosci.* 26, 360–368.
- Kleindienst, T., Winnubst, J., Roth-Alpermann, C., Bonhoeffer, T., and Lohmann, C. (2011). Activity-dependent clustering of functional synaptic inputs on developing hippocampal dendrites. *Neuron* 72, 1012–1024.
- Knott, G.W., Holtmaat, A., Wilbrecht, L., Welker, E., and Svoboda, K. (2006). Spine growth precedes synapse formation in the adult neocortex *in vivo*. *Nat. Neurosci.* 9, 1117–1124.
- Kwon, H.B., Kozorovitskiy, Y., Oh, W.J., Peixoto, R.T., Akhtar, N., Saulnier, J.L., Gu, C., and Sabatini, B.L. (2012). Neuroligin-1-dependent competition regulates cortical synaptogenesis and synapse number. *Nat. Neurosci.* 15, 1667–1674.
- Lai, C.S., Franke, T.F., and Gan, W.B. (2012). Opposite effects of fear conditioning and extinction on dendritic spine remodelling. *Nature* 483, 87–91.
- Larkum, M.E., and Nevanian, T. (2008). Synaptic clustering by dendritic signalling mechanisms. *Curr. Opin. Neurobiol.* 18, 321–331.
- Lee, K.J., Park, I.S., Kim, H., Greenough, W.T., Pak, D.T., and Rhyu, I.J. (2013). Motor skill training induces coordinated strengthening and weakening between neighboring synapses. *J. Neurosci.* 33, 9794–9799.
- Maletic-Savatic, M., Malinow, R., and Svoboda, K. (1999). Rapid dendritic morphogenesis in CA1 hippocampal dendrites induced by synaptic activity. *Science* 283, 1923–1927.
- Marco, E.J., Hinkley, L.B., Hill, S.S., and Nagarajan, S.S. (2011). Sensory processing in autism: a review of neurophysiologic findings. *Pediatr. Res.* 69, 48R–54R.
- Matsuzaki, M., Honkura, N., Ellis-Davies, G.C., and Kasai, H. (2004). Structural basis of long-term potentiation in single dendritic spines. *Nature* 429, 761–766.
- McAllister, A.K. (2007). Dynamic aspects of CNS synapse formation. *Annu. Rev. Neurosci.* 30, 425–450.
- Murakoshi, H., and Yasuda, R. (2012). Postsynaptic signaling during plasticity of dendritic spines. *Trends Neurosci.* 35, 135–143.
- Nägerl, U.V., Eberhorn, N., Cambridge, S.B., and Bonhoeffer, T. (2004). Bidirectional activity-dependent morphological plasticity in hippocampal neurons. *Neuron* 44, 759–767.
- Penzes, P., Cahill, M.E., Jones, K.A., VanLeeuwen, J.E., and Woolfrey, K.M. (2011). Dendritic spine pathology in neuropsychiatric disorders. *Nat. Neurosci.* 14, 285–293.
- Petersen, C.C. (2007). The functional organization of the barrel cortex. *Neuron* 56, 339–355.
- Rakic, P., Bourgeois, J.P., Eckenhoff, M.F., Zecevic, N., and Goldman-Rakic, P.S. (1986). Concurrent overproduction of synapses in diverse regions of the primate cerebral cortex. *Science* 232, 232–235.
- Rakic, P., Bourgeois, J.P., and Goldman-Rakic, P.S. (1994). Synaptic development of the cerebral cortex: implications for learning, memory, and mental illness. *Prog. Brain Res.* 102, 227–243.
- Redies, C., Hertel, N., and Hübner, C.A. (2012). Cadherins and neuropsychiatric disorders. *Brain Res.* 1470, 130–144.
- Saglietti, L., Dequidt, C., Kamieniarz, K., Rousset, M.C., Valnegri, P., Thoumine, O., Beretta, F., Fagni, L., Choquet, D., Sala, C., et al. (2007). Extracellular interactions between GluR2 and N-cadherin in spine regulation. *Neuron* 54, 461–477.
- Segal, M. (2005). Dendritic spines and long-term plasticity. *Nat. Rev. Neurosci.* 6, 277–284.
- Sheng, M., and Kim, E. (2011). The postsynaptic organization of synapses. *Cold Spring Harb. Perspect. Biol.* 3, a005678.
- Sheng, M., Sabatini, B.L., and Südhof, T.C. (2012). Synapses and Alzheimer's disease. *Cold Spring Harb. Perspect. Biol.* 4, a005777.
- Spacek, J., and Harris, K.M. (1997). Three-dimensional organization of smooth endoplasmic reticulum in hippocampal CA1 dendrites and dendritic spines of the immature and mature rat. *J. Neurosci.* 17, 190–203.
- Suarez, M.A. (2012). Sensory processing in children with autism spectrum disorders and impact on functioning. *Pediatr. Clin. North Am.* 59, 203–214, xii–xiii.
- Südhof, T.C. (2008). Neuroligins and neurexins link synaptic function to cognitive disease. *Nature* 455, 903–911.
- Tada, T., and Sheng, M. (2006). Molecular mechanisms of dendritic spine morphogenesis. *Curr. Opin. Neurobiol.* 16, 95–101.
- Tai, C.Y., Mysore, S.P., Chiu, C., and Schuman, E.M. (2007). Activity-regulated N-cadherin endocytosis. *Neuron* 54, 771–785.
- Tai, C.Y., Kim, S.A., and Schuman, E.M. (2008). Cadherins and synaptic plasticity. *Curr. Opin. Cell Biol.* 20, 567–575.
- Tan, Z.J., Peng, Y., Song, H.L., Zheng, J.J., and Yu, X. (2010). N-cadherin-dependent neuron-neuron interaction is required for the maintenance of activity-induced dendrite growth. *Proc. Natl. Acad. Sci. USA* 107, 9873–9878.
- Tanaka, H., Shan, W., Phillips, G.R., Arndt, K., Bozdagi, O., Shapiro, L., Huntley, G.W., Benson, D.L., and Colman, D.R. (2000). Molecular modification of N-cadherin in response to synaptic activity. *Neuron* 25, 93–107.
- Tang, G., Gudsnuik, K., Kuo, S.H., Cotrina, M.L., Rosoklja, G., Sosunov, A., Sonders, M.S., Kanter, E., Castagna, C., Yamamoto, A., et al. (2014). Loss of mTOR-dependent macroautophagy causes autistic-like synaptic pruning deficits. *Neuron* 83, 1131–1143.
- Trachtenberg, J.T., Chen, B.E., Knott, G.W., Feng, G., Sanes, J.R., Welker, E., and Svoboda, K. (2002). Long-term *in vivo* imaging of experience-dependent synaptic plasticity in adult cortex. *Nature* 420, 788–794.
- Turner, T.N., Sharma, K., Oh, E.C., Liu, Y.P., Collins, R.L., Sosa, M.X., Auer, D.R., Brand, H., Sanders, S.J., Moreno-De-Luca, D., et al. (2015). Loss of δ -catenin function in severe autism. *Nature* 520, 51–56.

- Xu, T., Yu, X., Perlik, A.J., Tobin, W.F., Zweig, J.A., Tenant, K., Jones, T., and Zuo, Y. (2009). Rapid formation and selective stabilization of synapses for enduring motor memories. *Nature* **462**, 915–919.
- Yang, G., Pan, F., and Gan, W.B. (2009). Stably maintained dendritic spines are associated with lifelong memories. *Nature* **462**, 920–924.
- Yu, X., and Malenka, R.C. (2003). Beta-catenin is critical for dendritic morphogenesis. *Nat. Neurosci.* **6**, 1169–1177.
- Yuste, R. (2013). Electrical compartmentalization in dendritic spines. *Annu. Rev. Neurosci.* **36**, 429–449.
- Yuste, R., and Bonhoeffer, T. (2004). Genesis of dendritic spines: insights from ultrastructural and imaging studies. *Nat. Rev. Neurosci.* **5**, 24–34.
- Zagrebsky, M., Holz, A., Dechant, G., Barde, Y.A., Bonhoeffer, T., and Korte, M. (2005). The p75 neurotrophin receptor negatively modulates dendrite complexity and spine density in hippocampal neurons. *J. Neurosci.* **25**, 9989–9999.
- Zheng, J.J., Li, S.J., Zhang, X.D., Miao, W.Y., Zhang, D., Yao, H., and Yu, X. (2014). Oxytocin mediates early experience-dependent cross-modal plasticity in the sensory cortices. *Nat. Neurosci.* **17**, 391–399.
- Zhou, Q., Homma, K.J., and Poo, M.M. (2004). Shrinkage of dendritic spines associated with long-term depression of hippocampal synapses. *Neuron* **44**, 749–757.
- Zoghbi, H.Y., and Bear, M.F. (2012). Synaptic dysfunction in neurodevelopmental disorders associated with autism and intellectual disabilities. *Cold Spring Harb. Perspect. Biol.* **4**, a009886.
- Zuo, Y., Lin, A., Chang, P., and Gan, W.B. (2005a). Development of long-term dendritic spine stability in diverse regions of cerebral cortex. *Neuron* **46**, 181–189.
- Zuo, Y., Yang, G., Kwon, E., and Gan, W.B. (2005b). Long-term sensory deprivation prevents dendritic spine loss in primary somatosensory cortex. *Nature* **436**, 261–265.

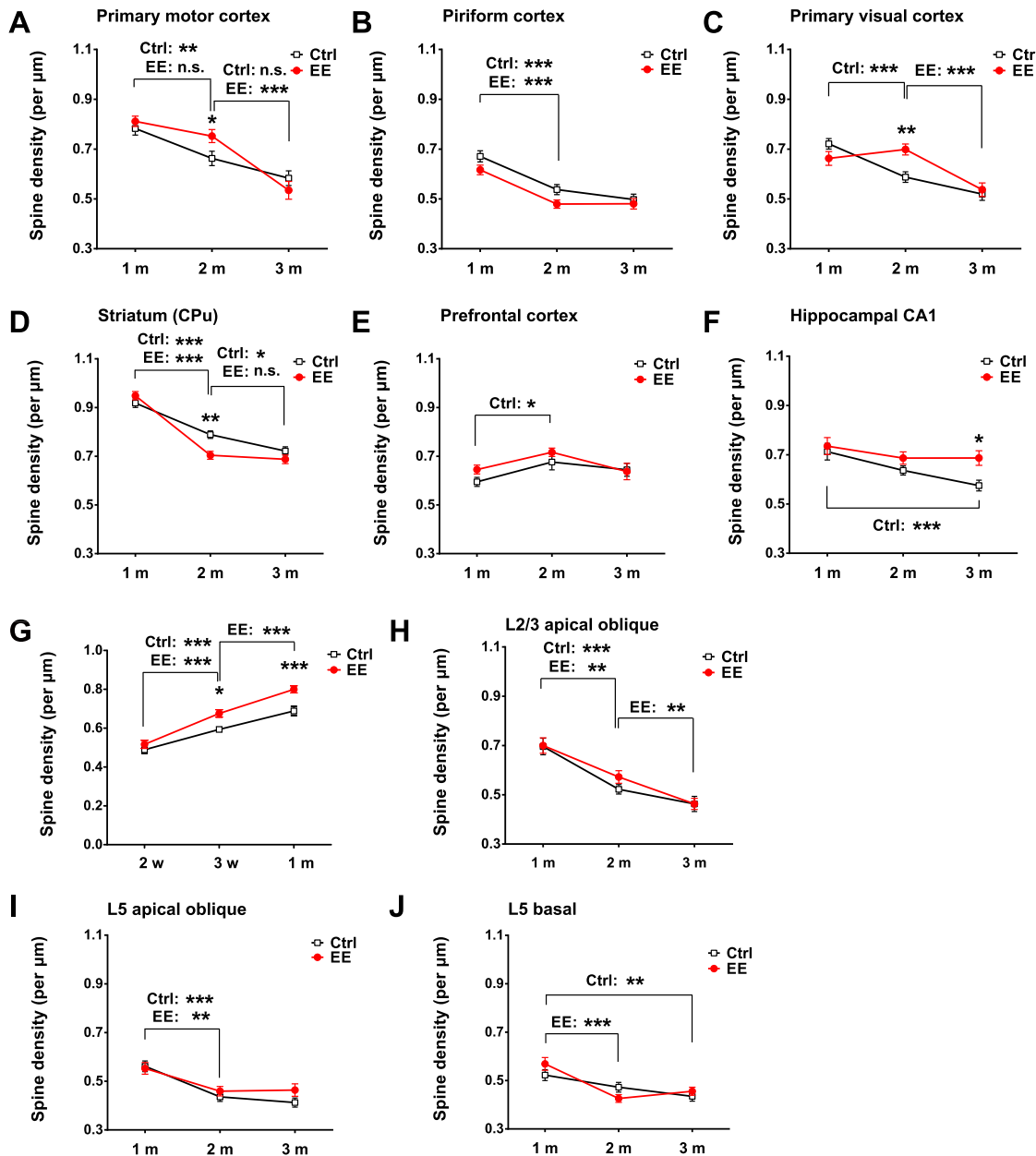


Figure S1. Spine Pruning Occurs in Multiple Brain Regions, Related to Figure 1

(A–F) Spine density of basal dendrites of layer 2/3 pyramidal neurons in primary motor cortex (A), piriform cortex (B), primary visual cortex (C), prefrontal cortex (E) and pyramidal neurons in hippocampal CA1 region (F), as well as spine density of medium spiny neurons in the dorsal striatum (D) in mice reared under Ctrl and EE conditions. (n = 27–50/group).

(G) EE promoted spinogenesis before 1 m in basal dendrites of S1BF layer 2/3 pyramidal neurons. (n = 39–46/group).

(H–J) The effect of EE on spine pruning in the apical oblique dendrites of layer 2/3 neurons or layer 5 neurons of S1BF. (n = 22–40/group). Data are presented as mean ± SEM. In this and all subsequent figures, error bars, SEM, *p < 0.05; **p < 0.01; ***p < 0.001; n.s.: p > 0.05.

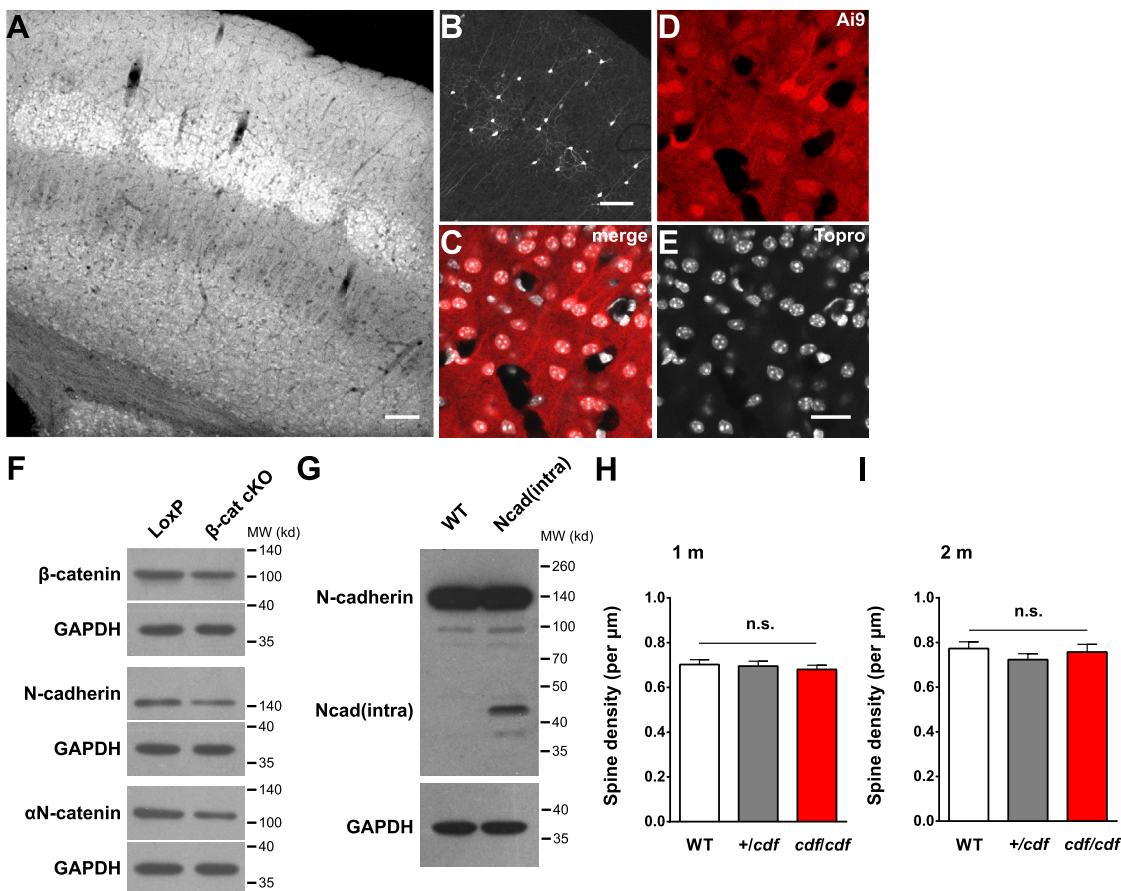


Figure S2. The Effect of Loss-of-Function of Components of the Cadherin/Catenin Complex on Spine Pruning, Related to Figure 2

(A and B) Fluorescent images showing tdTomato fluorescent signals in β -cat^{fl/fl};Ai9; CaMKCreERT2^{+/−} (β -cat cKO Ai9) mice injected with tamoxifen (A) or corn oil (B) from P27 to P31 and perfused on P36. Note the scattered Ai9 signals in corn oil injected mice (B), suggesting leaky expression of Cre in these mice.

(C–E) Brain slices of tamoxifen injected β -cat cKO Ai9 mice stained with the nuclear dye Topro.

(F) Western blots showing that the protein levels of β -catenin, N-cadherin and α N-catenin were reduced in 2 m β -cat^{fl/fl}; CaMKCreERT2^{+/−} (β -cat cKO) mice following tamoxifen injection at 1 m. The reduction of β -catenin, N-cadherin and α N-catenin levels are likely diluted by glial expression of β -catenin, which is not affected by tamoxifen-induced Cre expression.

(G) Western blots showing the expression of Ncad(intra), the intracellular domain of N-cadherin, in 1 m CaMKII α -Ncad(intra) mice.

(H and I) The spine density (n = 30–40/group) of layer 2/3 pyramidal neuron basal dendrites in S1BF of wild-type littermates, heterozygous and homozygous cdf mice.

Scale bars in (A) and (B) is 100 μ m; in C–E is 20 μ m. Data are presented as mean \pm SEM.

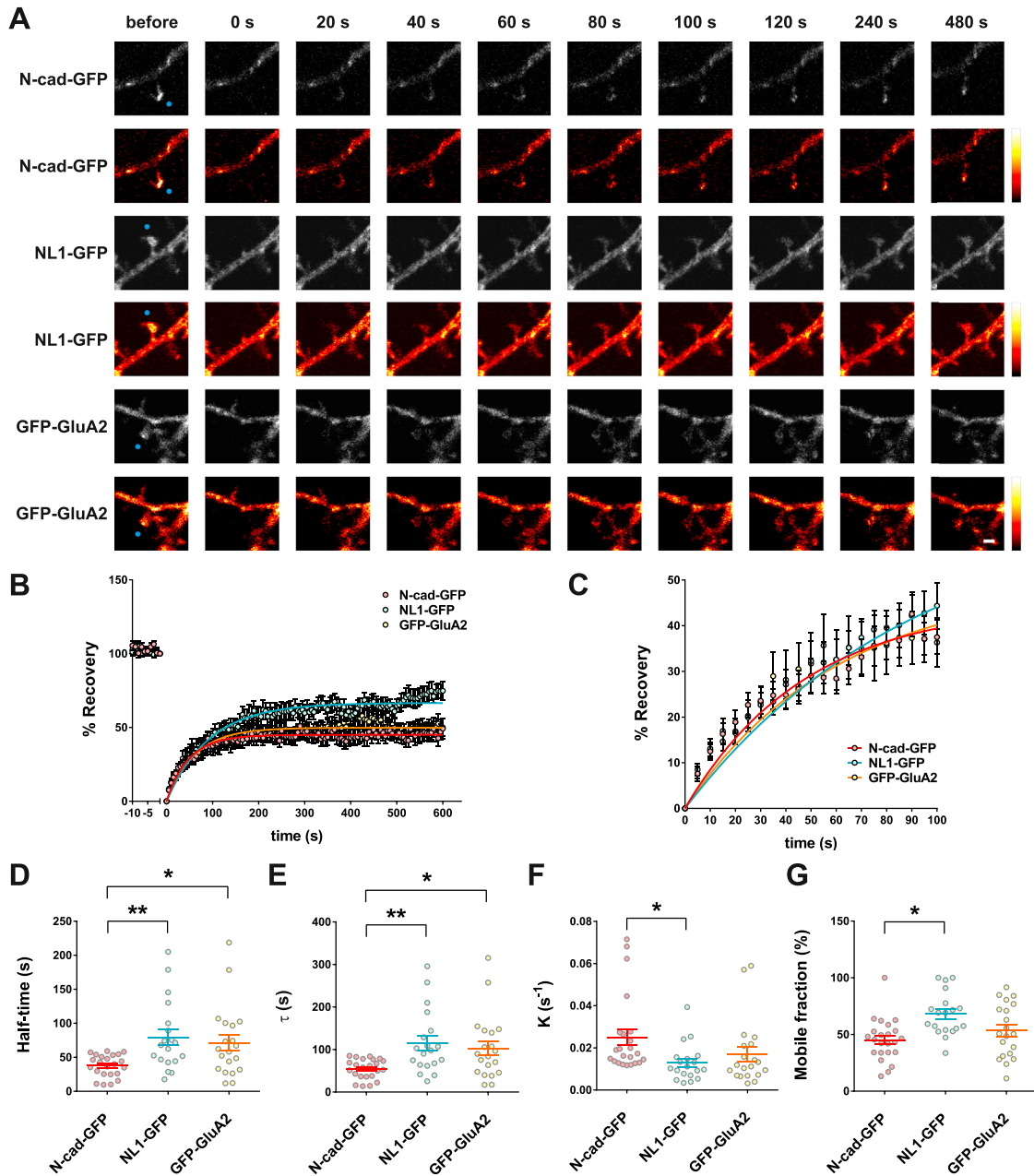


Figure S3. N-Cadherin Moves in and out of Spines Faster than Neuroligin-1 and GluA2, Related to Figure 4

(A) Representative images showing the fluorescence recovery after photobleaching (FRAP) of N-cad-GFP, NL1-GFP and GFP-GluA2 in spines. The time point immediately after photobleaching was defined as 0 s. Blue dots indicate the bleached spines. Scale bar, 1 μ m.

(B and C) Cell average data and one-exponential fit curves of the fluorescence recovery of N-cad-GFP, NL1-GFP and GFP-GluA2 ($n = 23$ spines for N-cad-GFP; 19 for NL1-GFP; 20 for GFP-GluA2; the FRAP curves of the first 100 s in B are magnified in C).

(D–G) Statistics showing the half-time, time constant τ , rate constant K and mobile fraction calculated from the FRAP curves of each spine. Data are presented as mean \pm SEM.

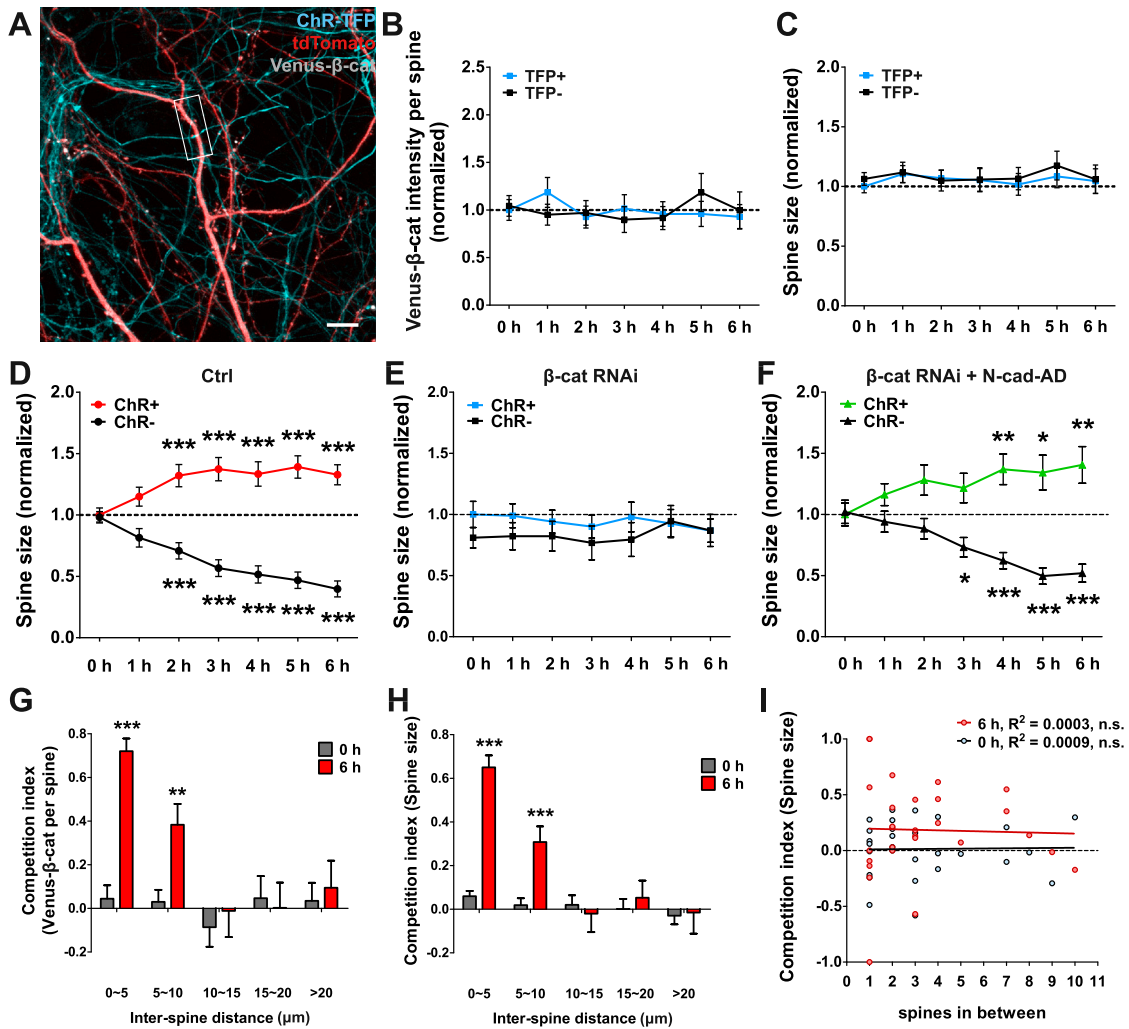


Figure S4. Activity Induces In Vitro Spine Fate Differentiation Requires β -Catenin-Dependent Adhesion and Depends on Inter-spine Distance, Related to Figure 5

(A) Representative image showing co-cultures containing ChR-TFP neurons (cyan) and neurons co-expressing tdTomato neurons (red) and Venus- β -cat (gray). Scale bar, 10 μ m. The box indicates the region of interest shown in Figure 5A as a representative example.

(B and C) Light stimulation did not induce Venus- β -cat redistribution (B) and spine fate differentiation (C) in spine pairs contacting TFP axons ($n = 64$, TFP+ versus TFP-: n.s. at all time points.).

(D-F) Spine size changes of spine pairs shown in Figure 5H under control (D, $n = 56$, ChR+ versus ChR-: n.s. at 0 hr, $p < 0.05$ at 1 hr, $p < 0.001$ at all other time points), β -cat RNAi (E, $n = 23$, ChR+ versus ChR-: n.s. at all time points) and β -cat RNAi + N-cad-AD rescue (F, $n = 34$, ChR+ versus ChR-: n.s. at 0–1 hr, $p < 0.05$ at 2 hr, $p < 0.01$ at 3 hr, $p < 0.001$ at all other time points) conditions.

(G and H) The increase in Venus- β -cat intensity (G) and spine size (H) CI induced by photostimulation is dependent on the distance between spine pairs. ($n = 41$ pairs in 0–5 μ m, 37 pairs in 5–10 μ m, 27 pairs in 10–15 μ m, 23 pairs in 15–20 μ m and 22 pairs in > 20 μ m, and including the $n = 58$ pairs shown in Figure 5D–5F).

(I) Spine size CI of pairs with inter-spine distance of 5–15 μ m in (A) and (B) were plotted against the number of spines in between at 0 hr ($n = 28$ pairs, not including those with no spines in between).

Data are presented as mean \pm SEM.

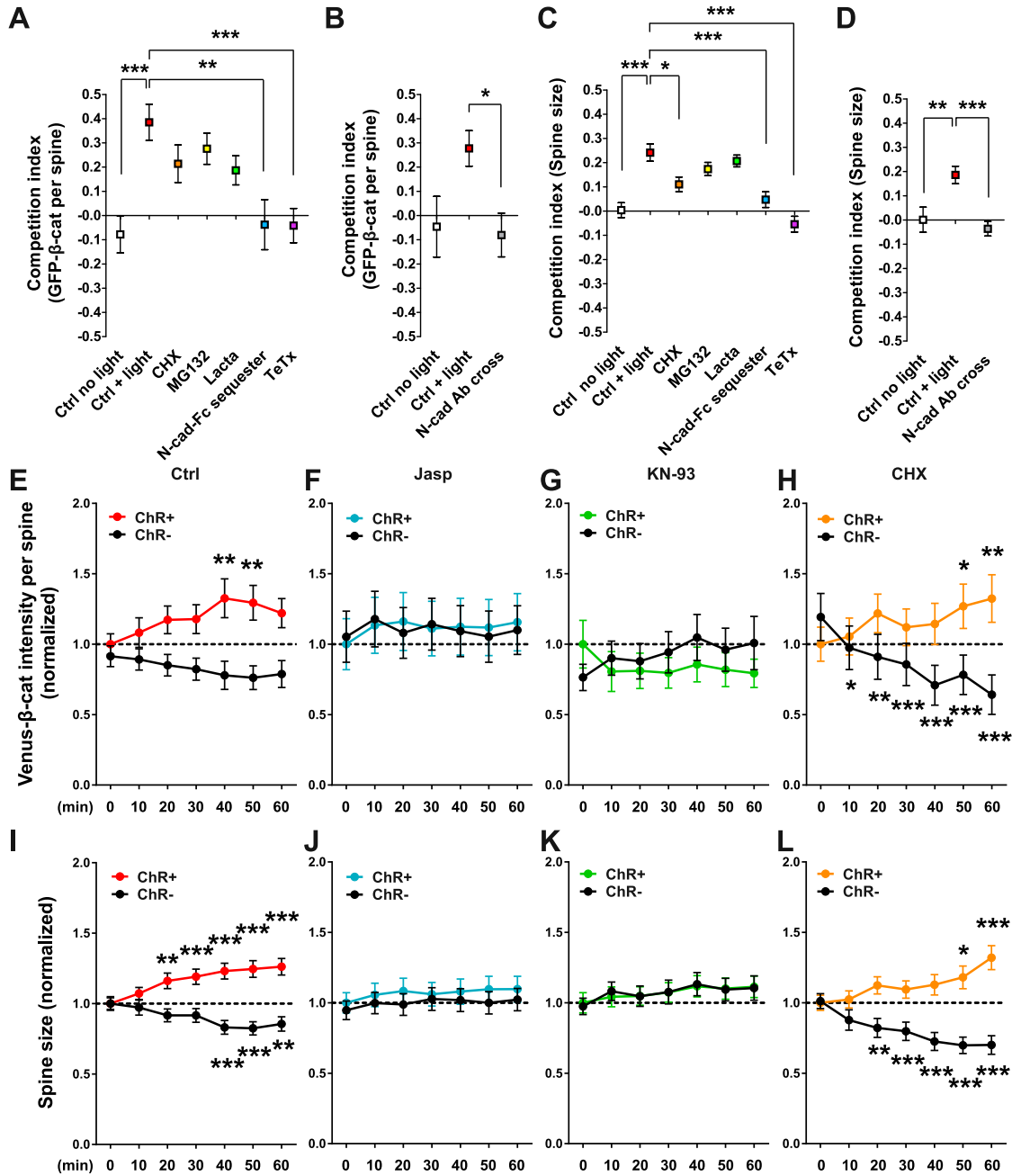


Figure S5. Activity-Induced Spine Fate Differentiation Depends on Synaptic Transmission, N-Cadherin Motility, Actin Reorganization, and CaMKII Activity, but Not Protein Synthesis or Degradation, Related to Figure 5

(A–D) ChR-tdTomato; CD8-HA + GFP- β -cat co-cultures were photo-stimulated for 8 hr and CI was calculated for each condition. CI change of either GFP- β -cat intensity (A and B) or spine size (C and D) induced by photo-stimulation was blocked by tetanus toxin (TeTx), and when dendritic N-cadherin were sequestered using N-cad-Fc beads (N-cad-Fc sequester) or crosslinked using antibodies against N-cadherin (N-cad Ab cross), but not in the presence of protein synthesis inhibitor cycloheximide (CHX) or proteosome inhibitors MG132 or lactacystin (Lacta, n = 51–83 pairs in A, C; n = 34–46 pairs in B, D for each condition).

(E–L) Live imaging of ChR-Teal; tdTomato + Venus- β -cat co-cultures at 10 min interval under photostimulation. PSA results showing changes in Venus- β -cat intensity (E – H) and spine size (I – L) between the spine pairs ($n = 104$ for Ctrl; 47 for Jasp; 68 for KN-93; 69 for CHX, ChR+ versus ChR-: E, 0 – 20 min, n.s., 30 min, $p < 0.05$, 40 – 50 min, $p < 0.001$, 60 min, $p < 0.01$; H, 60 min, $p < 0.001$, all others, n.s.; I, 0 – 30 min, n.s., 40 min, $p < 0.05$, 50 – 60 min, $p < 0.01$; L, 60 min, $p < 0.01$, all others, n.s.; F, G, J, K, n.s. at all time points).

Data are presented as mean \pm SEM.

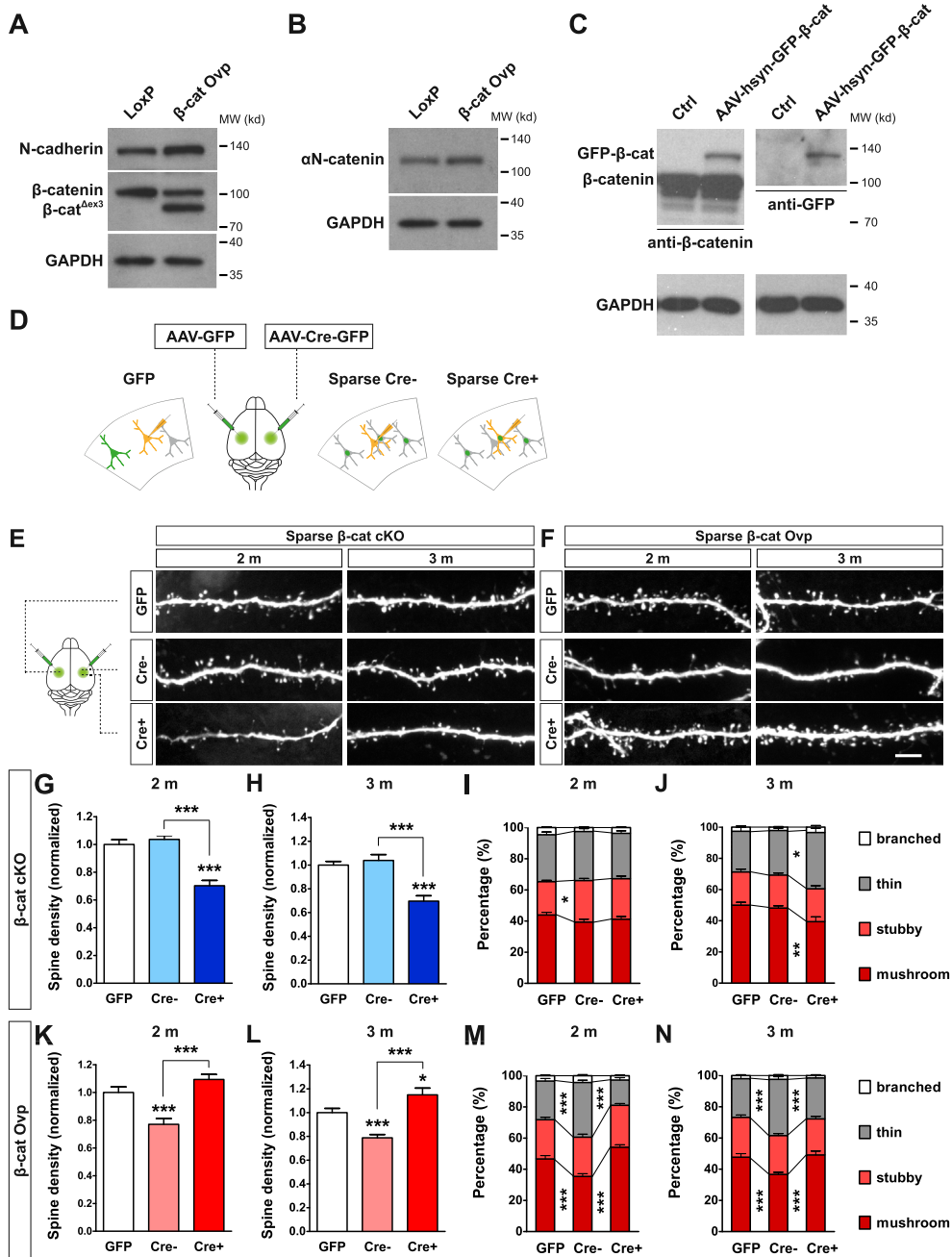


Figure S6. Altering Local β -Catenin Balance between Neighboring Neurons Biases Spine Pruning and Maturation In Vivo, Related to Figure 6

(A and B) Western blots showing expression of β -cat $^{\Delta ex3}$ (A, middle) in 1 m β -cat $^{\Delta ex3/\Delta ex3}$; NEX-Cre mice, as well as elevation in the protein levels of N-cadherin (A, top) and α N-catenin (B) in these mice.

(C) Western blots showing the expression of GFP- β -cat in cortex lysates from wild-type mice injected with AAV- GFP- β -cat (under human synapsin promoter). Left, GFP- β -cat and endogenous β -catenin were both detected by β -catenin antibodies; right, same lysates detected using GFP antibodies.

(D) Schematics showing bilateral AAV injection and grouping of GFP, Cre- and Cre+ neurons.

(E and F) Representative images of spines of GFP, Cre- and Cre+ neurons from β -cat $^{fl/fl}$ (E) or β -cat $^{\Delta ex3/\Delta ex3}$ (F) mice at 2 and 3 m following viral injection at 1 m.

(G–J) Spine density (G, 2 m; H, 3 m) and subtype distribution (I, 2 m; J, 3 m) of neurons in β -cat $^{fl/fl}$ mice ($n = 23–51$ /group).

(K–N) Spine density (K, 2 m; L, 3 m) and subtype distribution (M, 2 m; N, 3 m) of neurons in β -cat $^{\Delta ex3/\Delta ex3}$ mice ($n = 22–44$ /group).

Scale bars, 5 μ m. Data are presented as mean \pm SEM.

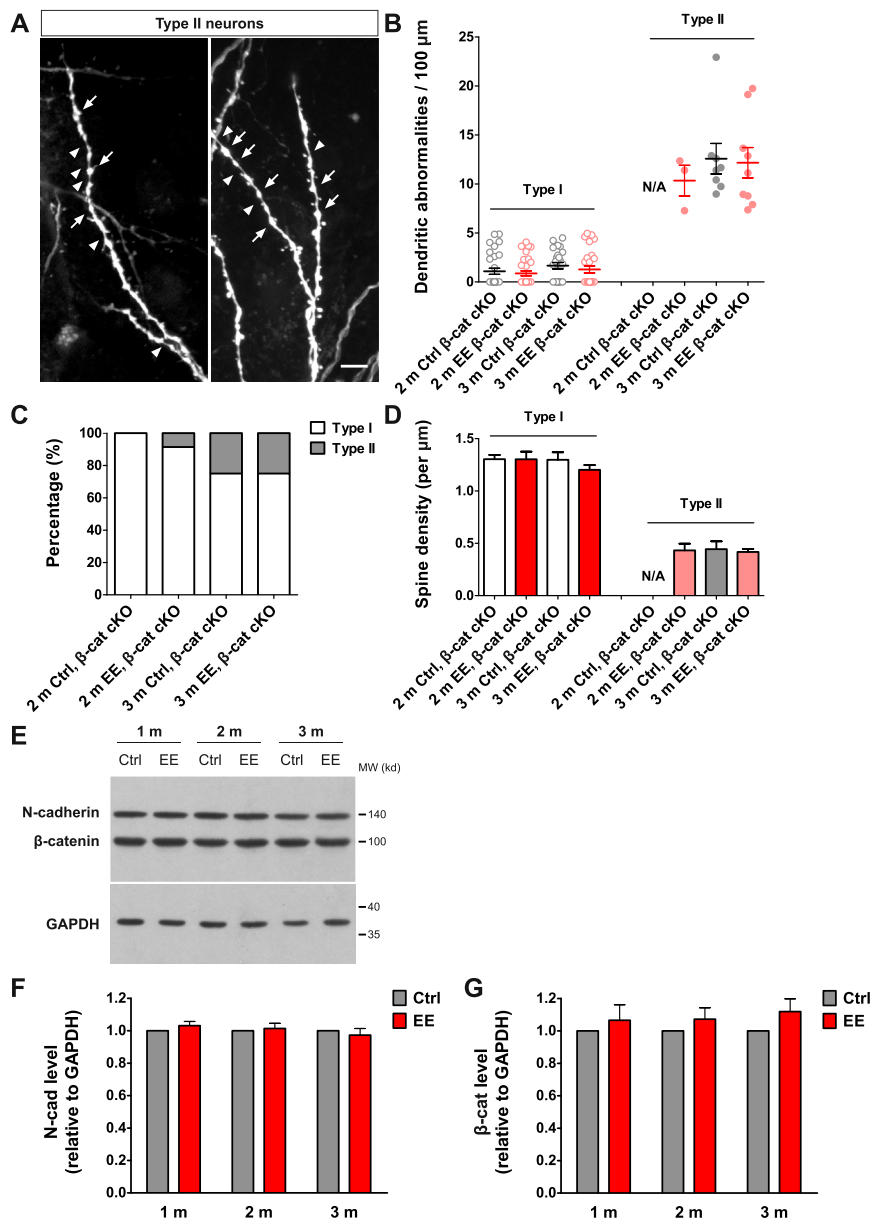


Figure S7. Characterization of Type I and Type II β -cat cKO Neurons and the Total Level of Cadherin/Catenin Complexes under Enrichment, Related to Figure 7

(A) Representative images showing the dendrites of lucifer yellow filled type II β -cat cKO neurons with severe dendritic abnormalities, including blebbing (arrows) and thinning (arrowheads). Scale bar, 5 μ m.

(B) Type II β -cat cKO neurons showed more severe dendritic abnormalities (blebbing + thinning) than type I β -cat cKO neurons.

(C) The occurrence frequency of type I and type II neurons in all conditions.

(D) The spine density in type I (same samples in Figures 7A–7D) and type II β -cat cKO neurons. In B and D, n = 3 in 2 m EE cKO, 8 in 3 m Ctrl cKO and 9 in 3 m EE cKO mice. Neurons with dendritic abnormalities of > 5 per 100 μ m were categorized as type II.

(E) Representative western blots showing the protein levels of N-cadherin and β -catenin in the cortices of Ctrl and EE mice.

(F and G) Quantification of the protein levels of N-cadherin and β -catenin (n = 4 animals per condition; paired t test between all Ctrl and EE pairs, n.s. for all pairs). Data are presented as mean \pm SEM.

Cell

Supplemental Information

**Coordinated Spine Pruning and Maturation
Mediated by Inter-spine Competition
for Cadherin/Catenin Complexes**

Wen-Jie Bian, Wan-Ying Miao, Shun-Ji He, Zilong Qiu, and Xiang Yu

Supplemental Experimental Procedures

Animals

All animal procedures complied with the animal care standards set forth by the US National Institutes of Health and have been approved by the Institutional Animal Care and Use Committee of the Institute of Neuroscience, Chinese Academy of Science (Shanghai, China). The β -catenin conditional knockout (cKO) mice (β -*cat*^{f/f}; full name: B6.129-*Ctnnb1*^{tm2Kem}/KnwJ; JAX strain 004152)(Brault et al., 2001), *cerebellar deficient folia* spontaneous mutant mice (*cdf*; full name: C3Sn.C3-*Ctnna2*^{cdf}/J; JAX strain 002235, C3H background)(Park et al., 2002), Ai9 mice (full name *B6.Cg-Gt(ROSA)26Sor*^{tm9(CAG-tdTomato)Hze}/J; JAX strain 007909) and Ai34D mice (full name *B6;129S-Gt(ROSA)26Sor*^{tm34.1(CAG-Syp/tdTomato)Hze}/J; JAX strain 012570) were obtained from the Jackson Laboratory (U.S.A.). Conditional expression of stabilized β -catenin was achieved using the *Catnb*^{lox(ex3)} (β -*cat*^{Aex3}) mice, in which exon 3 of β -catenin, containing multiple serine/threonine phosphorylation sites regulating its degradation, is flanked by loxP sites (Harada et al., 1999) (gift of Prof. Makoto M. Taketo, Kyoto University, Japan). The *CaMKII α -Ncad(intra)* mice expressed Ncad(intra) (Yu and Malenka, 2003), the intracellular domain of N-cadherin, under a CaMKII α promoter (Abel et al., 1997) (promoter construct gift of Dr. Yizheng Wang, Institute of Neuroscience, SIBS, Shanghai, China). Targeting vector was generated by He-Ling Song (Institute of Neuroscience, SIBS, Shanghai, China) and transgenic mice were generated by the Transgenic Core Facility of the Institute of Neuroscience.

The *NEX-Cre* mice (Goebels et al., 2006) expressed Cre in excitatory neurons of the cerebral cortex and hippocampus starting from the late embryo (gift of Prof. Klaus Nave, Max Planck Institute, Goettingen, Germany). The *CaMKCreERT2* mice (full name: Tg(*Camk2a-cre/ERT2*)2Gsc) (Erdmann et al., 2007) are BAC transgenic mice expressing Cre in excitatory neurons of the cerebral cortex and hippocampus upon tamoxifen injection (obtained from the European Mouse Mutant Archive, Germany; EM: 02125). In all experiments, β -*cat*^{f/f} or β -*cat*^{Aex3/Aex3} mice were homozygous, while Cre drivers were heterozygous. Homozygous LoxP littermates not expressing the Cre driver were used as controls, except for experiments in Fig. 6, where Ai34D mice without β -*cat*^{Aex3/Aex3} alleles

were used as controls. For inducible Cre expression, one-month-old β -cat^{f/f}; CaMKCreERT2 mice were intraperitoneally injected with tamoxifen (Sigma, T5648, dissolved in corn oil) at 50 µg/g body weight/d for 5 consecutive days. Due to leaky basal expression of CaMKCreERT2 (Fig. S2B), negligible before 1m but increasing with mouse age, we used floxed littermates (β -cat^{f/f}; LoxP control) injected with tamoxifen as controls. All mice were on C57BL/6 background, except for *cdf* mutants, which were kept on C3H background.

Environment enrichment and whisker deprivation

The environment enrichment (EE) paradigm was as previously described (He et al., 2010; Zheng et al., 2014). Briefly, C57BL/6 pregnant mice (2 for enrichment, 1 for standard control) were randomly assigned to standard Ctrl (32.5 cm × 21 cm × 18.5 cm cages) or EE (50 cm × 36 cm × 28 cm cages) housing 1-4 days before delivery. The EE cages contained objects of various shapes and textures, repositioned daily and completely substituted once per week. Ctrl cages had a maximum of 5 mice during the entire experiment. For the EE cages, since the same cage was assayed at 3 time points, and a minimum of 8 mice was needed at all times to ensure increased social interactions, some EE cages were pooled before 1 m. For whisker deprivation, 2-month-old mice reared in standard cages were anaesthetized using isoflurane, and all whiskers on one side were trimmed every 5 days while the other side remained intact as an internal control. All mice were kept under a 12 h-12 h light-dark cycle with food and water provided *ad libitum* from the cage lid. Only male mice were used, except for those of 1 month or younger, to avoid the potential influence of the oestrus cycle on spine density (Woolley and McEwen, 1993).

Golgi staining

Age-matched Ctrl and EE mice were deeply anaesthetized with 0.14g/kg sodium pentobarbital. Brains were quickly removed and Golgi staining was performed using the FD Rapid GolgiStain™ Kit (FD NeuroTechnologies, PK401), according to the manufacturer's instructions. At least 3 mice from 2 different litters were used per time

point.

Viral injections

P28–30 mice were anesthetized with sodium pentobarbital (0.07g/kg), and adeno-associated viruses (AAVs, packaged by Obio Technology, Shanghai, China) was injected into the S1BF as previously described (Zheng et al., 2014). For high density infection, 1.5 μ l AAV-Cre-GFP (Lu et al., 2009) (construct gift of Dr. Wei Lu, National Institutes of Health, Bethesda, MD, USA; 1×10^{12} TU/ml) or AAV-GFP (AAV backbone and human synapsin promoter from Addgene plasmid 26976; 1×10^{12} TU/ml) was injected into the S1BF at a speed of 0.1 μ l/min and a depth of 300 μ m. For sparse infection, 1 μ l of the virus, diluted 5-10 fold, was injected. For the experiments in Fig. 6, 0.3–0.5 μ l AAV-Cre-GFP (human synapsin promoter; 1×10^{13} TU/ml), diluted 10 fold, or 0.5 μ l AAV- β -cat-GFP (human synapsin promoter; 1×10^{12} TU/ml), diluted 10 fold, were respectively injected at 2 neighboring sites within S1.

Immunohistochemistry and fluorescent dye microinjections

Viral injected mice were deeply anaesthetized with 0.14g/kg sodium pentobarbital and perfused with pre-warmed phosphate buffered saline (PBS), followed quickly with 4% paraformaldehyde (PFA, Sigma-Aldrich, St. Louis, MO, USA) in phosphate buffer. The brains were dissected and post-fixed in 4% PFA for 4 h. For immunohistochemistry, the brains were equilibrated in 30% sucrose and coronally sectioned at 30 μ m as previously described (Zheng et al., 2014). For infection rate validation, the following antibodies and dyes were used: CamKII β (Abcam, ab34703, rabbit, 1:1000), Alexa-Fluor 568 (Invitrogen, A11036, goat anti-rabbit, 1:1000) and NeuroTrace 640/660 (Invitrogen, N-21483, 1:1000). For PSA of β -catenin level *in vivo*, GFP (Invitrogen, rabbit, A11122, 1:1000,) and Alexa-Fluor 488 secondary antibodies (Invitrogen, A11034, goat anti-rabbit, 1:1000) were used to amplify β -cat-GFP signals. For fluorescent dye microinjections (Belichenko et al., 2004; Wallace and Bear, 2004), the post-fixed brains were stored in 4°C PBS and coronally sectioned at 250 μ m slices using a Leica VT1200S Vibratome (Germany). Injections were carried out under a 40 \times water immersion objective on a Nikon FN1

fluorescence microscope (Japan). Sharp glass pipettes (resistance 80–120 MΩ) were loaded with an aqueous solution of 6% (w/v) lucifer Yellow CH Lithium Salt (LY, Invitrogen, L-453) or 4 mM Alexa Fluor 488 Carboxylic Acid (Invitrogen, A20000) and targeted to the cell bodies of layer 2/3 pyramidal neurons using a micromanipulator (Sutter instruments, CA, USA). Cells were visualized under DIC, and AAV-Cre-GFP infected neurons were identified by nuclear Cre-GFP fluorescence. Upon pipette penetration, the cell body and proximal dendritic shafts of the target neuron were instantly filled with the fluorescent dye, allowing identification of pyramidal neurons by their triangular somata and distinct apical dendrites. The dye was further iontophoretically injected at a constant current of -2 nA or -5 nA, at on/off cycles of 2 Hz for 5 min (MultiClamp 700B amplifier, Molecular Devices, CA, USA), until all dendrites and spines were fully filled with bright fluorescence. All sections were mounted in 75% glycerol.

Hippocampal neuronal culture and constructs

Primary dissociated hippocampal cultures were prepared from P0 rat pups as previously described (Tan et al., 2010; Yu and Malenka, 2003). Briefly, dissociated hippocampal neurons were plated on matrigel-coated (BD Bioscience, San Jose, CA, USA) 35 mm glass bottom μ-Dishes (Ibidi, 81158, Martinsried, Germany) at 70,000 cells/cm², in Neurobasal medium (Invitrogen, Carlsbad, CA, USA) containing B-27 (Invitrogen, Carlsbad, CA, USA), 2 mM Glutamax-I (Invitrogen, Carlsbad, CA, USA), and 2.5% FBS (HyClone, Logan, UT, USA).

In terms of constructs, GFP-β-cat was as previously described (stabilized form, originally named GFP-β-cat*) (Yu and Malenka, 2003); Venus-β-cat was generated by replacing GFP with Venus, a yellow-shifted form of GFP (Nagai et al., 2002); pH-N-cad was generated by inserting pHluorin, a pH-sensitive form of GFP (Miesenbock et al., 1998), into the extracellular domain of mouse N-cadherin, between residues 310 and 311, according to a previous report (Kim et al., 2011). GFP-β-cat, Venus-β-cat and pH-N-cad were subcloned into pCS2min, a modified pCS2 vector that overexpressed proteins in an activity-independent manner (Tan et al., 2010). AAV-GFP-β-cat was generated under the

human synapsin promoter. ChIEF (Lin et al., 2009) (gift of Prof. Roger Tsien, UC San Diego, CA, U.S.A.) is a modified form of Channelrhodopsin (ChR), suitable for high frequency, repeated stimulation. It was expressed under the CAG promoter, either fused to tdTomato or Teal fluorescent protein (Hirani et al., 2013) (TFP, blue-shifted GFP, Addgene Plasmid 42147: pNH013). pCMV5-Neuroligin1-EGFP (Chubykin et al., 2007) (NL1-GFP) was a gift of Prof. Thomas Südhof (Stanford University, USA). N-cad-GFP (gift of Dr. Chin-Yin Tai, Academia Sinica, Taiwan), with GFP fused into the C-terminus of mouse N-cadherin, and GFP-GluA2 (gift of Dr. Hailan Hu, Institute of Neuroscience, SIBS, CAS) (Shi et al., 2001) with GFP fused to the N-terminus of rat GluA2 immediately after the signal peptide, were subcloned into pCS2 or pCAG. N-cad-AD is a chimeric molecule consisting of the extracellular and transmembrane domains of N-cadherin fused to the actin-binding domain of α N-catenin and functionally replaces loss-of-function of any component of the cadherin/catenin complex (Tan et al., 2010). N-cad-AD, β -catenin RNAi and CD8-HA constructs were as previously described (Bian et al., 2015; Tan et al., 2010).

For beads experiment, constructs encoding GFP- β -cat, pH-N-cad, or NL1-GFP were co-transfected with plasmids encoding the morphology marker tdTomato at days *in vitro* (DIV) 9 using calcium phosphate transfection. For light stimulation experiments, 120,000 cells/cm² neurons were electroporated (Nucleofector II; Amaxa, Cologne, Germany) with ChR or TFP control constructs at the time of plating, together with 30,000 cells/cm² unelectroporated neurons. Approximately 10-30% of neurons expressed ChR. The cultures were subsequently transfected at low efficiency (< 1%) using calcium phosphate on DIV9 with constructs needed for analysis of postsynaptic spines (tdTomato + Venus- β -cat for tri-color live imaging, GFP + appropriate plasmids for RNAi and rescue for RNAi experiments or CD8-HA + GFP- β -cat for fixed sample experiments). Since electroporation and transfection were performed independently and at different times, distinct populations of neurons were transfected (visualized by expression of distinct fluorescent proteins), allowing for selection of juxtaposing presynaptic ChR termini and postsynaptic spines. On the rare occasions when neurons were transfected with both ChR and td-Tomato/GFP constructs, they were excluded from subsequent experiments. All live

imaging experiments were carried out at DIV 16.

Beads coating

Polystyrene carboxylated beads (2 µm in diameter, 18327; Polysciences, Marrington, PA, USA) were covalently coated with recombinant proteins according to previously described methods (Zhang and Poo, 2002). Briefly, carboxylated beads were rinsed with 0.1 M carbonate buffer (pH 9.6), 0.02 M phosphate buffer (pH 4.5) and pretreated with 1% EDAC (1-ethyl-3-(3-dimethylaminopropyl)-carbodiimide hydrochloride; Sigma, St. Louis, MO, USA) in phosphate buffer (pH 4.5) at room temperature for 3 h. After washing in 0.2 M borate buffer (pH 8.5), the beads were incubated with either N-cadherin-Fc (20 µg/ml, 1388-NC-050, residues 160-724 of human N-cadherin fused to residues 100-300 of human IgG1; R&D Systems, Minneapolis, MN, USA), Neurexin-1β-Fc (20 µg/ml, 5268-NX-50, residues 51-362 of human Neurexin-1β fused to residues 100-300 of human IgG1; R&D Systems, Minneapolis, MN, USA), or human Fc (20 µg/ml, 110-HG; R&D Systems, Minneapolis, MN, USA) in borate buffer at 4°C overnight. The coated beads were pelleted, blocked with 1% bovine serum albumin (BSA; Calbiochem, San Diego, CA, USA) and stored in 0.02 M phosphate buffer containing 0.88% NaCl, 1% BSA and 5% glycerol (pH 7.4) at 4°C. Protein concentration in the supernatant was measured to confirm coating efficiency. Successful coating was verified using primary antibodies against the human Fc fragment (Jackson ImmunoResearch, 109-005-098, goat anti-human, 1:2000) and Alexa-488 secondary antibodies (Invitrogen, A11055, donkey anti-goat, 1:1000).

Image acquisition and live imaging

For Golgi staining experiments, basal dendrites of layer 2/3 pyramidal neurons in the S1BF (or other neurons and brain regions as indicated) were imaged at 1 µm Z intervals on a Zeiss LSM PASCAL confocal microscope (Carl Zeiss, Jena, Germany), using a 63× oil immersion Plan-Apochromat objective (N.A. = 1.4) and 2× optical zoom. Images for infection rate validation were also acquired on the same system using a 40× oil immersion Neofluor objective (N.A. = 1.3). For dye-microinjected brain slices and experiments in

Fig. 6, basal dendrites of neurons were imaged on a Nikon A1 confocal microscope (Nikon, Tokyo, Japan) with a Plan Apo VC 60x Oil DIC N2 objective (N.A. = 1.4), at 3× optical zoom and 0.3 μm Z intervals.

Live imaging experiments was performed on a Nikon A1R confocal microscope (Nikon, Tokyo, Japan) or Olympus FV10i confocal microscope (Olympus, Tokyo, Japan). DIV16 neurons plated in 35 mm glass-bottom dishes were maintained at 37°C in a Stage Top Incubator (Tokai Hit, Japan), and images were acquired with a Nikon Plan Apo VC 60× Oil DIC N2 objective (N.A. = 1.4) or an Olympus UPLSAPO60× water immersion objective (N.A. = 1.2) at 2× optical zoom and 1 hour interval. The neuron was imaged at 1 μm Z intervals. For beads experiments, protein-coated beads were applied to the cultures 30 min before imaging to allow the beads to sink to the bottom of the dish. For light stimulation experiments, a custom-made LED system (gift of Dr. Yunqing Wen, Institute of Neuroscience, SIBS, CAS) controlled by Master-8 (A. M. P. I., Israel) was used to stimulate cultures with a train of blue light (~470 nm) pulses every 60 s. Each train consisted of 10 pulses at 4 Hz, with each pulse lasting for 10 ms. 0.5 μM tetrodotoxin (TTX, Fisheries Science and Technology Development, Hebei, China) was add to the medium prior to light stimulation to block recurrent action potentials, without affecting light evoked depolarization and synaptic transmission (Zhang and Oertner, 2007). For live imaging within 1 h, single plane images were collected every 10 min and the light train was applied every 30 s. Jasplakinolide (Jasp, Invitrogen, J7473, 1 μM), KN-93 (Sigma, K1385, 10 μM) or cycloheximide (CHX, Sigma, C4859, 50 $\mu\text{g/ml}$) was added to the medium together with 0.5 μM TTX, prior to the stimulation.

For fixed sample experiments, light stimulation was delivered every 60 s with the above protocol for 8 h. The following reagents was added to the medium together with 0.5 μM TTX prior to the stimulation, 50 $\mu\text{g/ml}$ CHX, MG132 (Tocris, 1748, 10 μM), lactacystin (lacta, Millipore, 426100, 10 μM), tetanus toxin (TeTx, Sigma, T3194, 2 $\mu\text{g/ml}$), N-cad-Fc coated beads or antibodies against the extracellular domain of N-cadherin (Abmart, 448-1-1/844-1-2(2#3#)3A3, mouse, 1:250). At the end of light stimulation, neurons were fixed in 4% PFA, permeabilized in 0.1% Triton-X100, blocked with 3% BSA and incubated with primary antibodies against HA tag (Abmart, M20003,

mouse, 1:1000) and GFP (Invitrogen, A11122, rabbit, 1:1000), followed by the corresponding secondary antibodies (Alexa-Fluor 633, A21052, goat anti-mouse; Alexa-Fluor 488, A11034, goat anti-rabbit, Invitrogen, 1:1000). Images were acquired at 1 μ m Z intervals on a Zeiss LSM PASCAL confocal microscope (Carl Zeiss, Jena, Germany), using a 63 \times oil immersion Plan-Apochromat objective (N.A. = 1.4) and 2 \times optical zoom.

For all culture experiments, at least 2 independent culture preparations were used per experimental condition, and all bead experiments were interleaved with control experiments using Fc beads.

Fluorescence recovery after photobleaching (FRAP)

FRAP experiments and data analyses were performed according to previous studies (Ashby et al., 2006; Saglietti et al., 2007; Sharma et al., 2006; Tai et al., 2007) and with some modifications. Briefly, DIV 16 cultured neurons was placed in a Stage Top Incubator (Tokai Hit, Japan) at 37°C and under a Nikon A1R confocal microscope (Nikon, Tokyo, Japan). Time-series of single plane images were acquired with a Nikon Plan Apo VC 60 \times Oil DIC N2 objective (N.A. = 1.4) at 12 \times optical zoom, at 1 s intervals pre-bleaching and 5 s intervals post-bleaching. The target spine was photobleached by scanning the region of interest using the maximum power of 488 nm laser at 4 Hz 4-8 times. Images were analyzed using Fiji/ImageJ (NIH, Bethesda, MD, USA). For each image, the total intensity of a region of interest covering the bleached spine was measured and background intensity subtracted. The mean intensity of a distant, unbleached dendritic region was used to compensate overall bleaching caused by image acquisition. To normalize data from different experiments, the pre-bleaching intensities were set to 100% and immediate post-bleaching intensities to 0%. Each set of recovery measurements were fit using GraphPad Prism 5 (GraphPad software) with the single exponential equation: %Recovery = $(1 - e^{-Kt}) \cdot 100\%$, where t is the time past bleaching and K is the rate constant for recovery. Other parameters were calculated as follows: Half-time = $\ln(2)/K$, defined as the time required to recover half way between initial and steady-state fluorescence intensities; time constant $\tau = 1/K$; and the mobile fraction equals

the percentage recovery when the curve plateaus.

Image analysis

For all morphological analyses, images were coded using computer-generated random number sequences at the time of data acquisition and all analyses were performed blinded to the experimental condition.

For Golgi staining and fluorescent dye microinjection Z-stack images, dendritic branches were traced using the Simple Neurite Tracer plugin in Fiji/ImageJ (NIH, Bethesda, MD, USA) and every spine on the branch was counted using ImageProPlus (Media-Cybernetics, Silver Spring, MD, USA). Spine density was calculated by dividing the total spine number by the dendritic branch length. Protrusions longer than 5 μm were considered as filopodia and excluded from the analysis. For dye-fill experiments, spine density was normalized among mice of the same litter, to the control condition of the first time point (usually 1 month). Spine head diameter, spine neck diameter, spine length and inter-spine distance were semi-automatically measured using ImageProPlus. Spine subtypes were classified based on previously defined morphological criteria (Harris et al., 1992; Zagrebelsky et al., 2005) and quantitated as follows: a) mushroom: the spine head diameter is $\geq 1.5 \times$ the diameter of spine neck ($d_h/d_n \geq 1.5$); b) stubby: head and neck of the spine are approximately of same width, and spine length is not significantly longer than the head diameter ($d_h/d_n < 1.5$, $L/d_h < 2$); c) thin: diameters of spine head and neck are nearly equal, and spine length is greater than spine width ($d_h/d_n < 1.5$, $L/d_h \geq 2$); and d) branched: spines with more than one head. Only images (blind-coded) with sufficient quality to clearly identify and measure spine shapes were used in the subtype classification, and 20–30 consecutive spines on the same dendrite were analyzed per image. To calculate viral infection rate, total number of Nissl-positive cell bodies, as well as neuronal cell bodies containing Cre-GFP and/or CamKII β signals, were counted using ImageProPlus.

All images were analyzed as acquired with no post-acquisition modifications. For Golgi staining example images, bright-field Z-stack images were projected at minimal intensity and inverted, background was then subtracted, followed by brightness/contrast

adjustment within linear ranges, using Fiji/ImageJ (NIH, Bethesda, MD, USA). For fluorescent image and western blots examples, brightness/contrast adjustment within linear ranges were made using Fiji/ImageJ when necessary. For images in Fig. 6D, I and supplementary movies, Z-stack images were deconvolved using Huygens Essential (SVI, Laapersveld Hilversum, Netherlands) (Schoonover et al., 2014), and 3D rendering was achieved in Imaris (Bitplane, Zurich, Switzerland) using the deconvolved images. Control and experiment conditions were adjusted with the same parameters.

For imaging cultured neurons, Paired Spines Analysis (PSA) was performed using projected Z-stacks images (for bead or 6-hour ChR experiments) or single plane images (for 1 h ChR experiments) with ImageProPlus. Neighboring spines (regions of interest) on the same dendritic branch were manually outlined from images in the tdTomato (or other morphology markers) channel and thresholded. A mask was then generated and used to measure spine area and total intensity of GFP- β -cat and/or various fluorescently-tagged proteins. The identity of spines was verified through all frames of the time series using morphological landmarks within the images, as well as positions of the beads and/or ChR axons. Experiments were only included in the analyses if analyzable images were obtained for all time frames, and the relationship of the spine with respect to the bead or ChR axon remained constant throughout the experiment: i.e. the bead+ spine was in contact with a bead in all image frames and the bead- spine not contacting any beads in all image frames; for ChR experiments, the ChR axon was in contact with the ChR+ spine for all image frames, while the ChR- spine was not in contact with any ChR axon. The competition index (CI) was calculated as: $(pC^+ - pC^-)/(pC^+ + pC^-)$, in which “p” is the parameter of interest, i.e. spine size or integrated intensity of the fluorescently-tagged molecule and “C⁺” or “C⁻” indicates whether the parameter was measured in a contacting (C⁺) or non-contacting (C⁻) spine, be it bead or ChR axon. In rare cases when the two spines within a pair both disappeared, CI was defined as “0”. In PSA results shown in Fig. 3, 4B, C, G, H, 5D-F, H, and S4B-F, only spine pairs fulfilling the following criteria were analyzed: 1) within 10 μ m of each other, 2) with no spines in between them at 0 h, and 3) at least one of them survived through all image frames. In Fig. 4E, 5G and S4G-I, additional pairs with inter-spine distance ≥ 10

μm and/or with in-between spines ≥ 1 at 0 h were added to the data pool, regardless their survival status.

In fixed sample experiments using N-cad-Fc beads (N-cad-Fc sequester, Fig. S5A, C), beads were used to sequester N-cadherin away from spines of interest. Thus the analyzed ChR+/ChR- spine pairs did not contact beads themselves, while the dendrite segment on which the spines are located, as well as other neighboring spines were in contact with beads.

For *in vivo* comparison of Ai+ and Ai- spines, PSA was performed on projected Z-stacks images by choosing an Ai+ spine and the nearest Ai- spine (regions of interest) on the same dendritic branch, and spine area or total GFP- β -cat intensity was thresholded and measured using ImageProPlus. A circle of radius 10 μm was then drawn around the Ai+ spine, and every Ai+ and Ai- spine within that circle and on the same dendritic branch, as well as Ai puncta co-localizing with the dendrite/spine were counted using ImageProPlus. The sizes of Ai+/Ai- spine pairs were normalized to the mean size of all the spines measured in that circle, and the intensity of GFP- β -cat was normalized to the mean intensity of all spines analyzed on the same neuron (usually 6-10 spines).

Western blots

Wild-type mice reared under standard and EE conditions, wild-type mice injected with AAV-GFP- β -cat viruses at 1 month, *NexCre*^{+/−}; β -cat^{Δex3/Δex3} mice, *CaMKCreERT2*^{+/−}; β -cat^{f/f} mice injected with tamoxifen at 1 month and control littermates were deeply anaesthetized with 0.14g/kg sodium pentobarbital. Cortices were dissected and homogenized, and the membrane fraction was prepared as previously described (He et al., 2010). Western blot was performed according to standard protocols, and results were quantified using ImageJ software (NIH Image). The following primary antibodies were used: N-cadherin (mouse, Invitrogen, 33-3900, 1:3000), β -catenin (mouse, BD Biosciences, 610154, 1:3000), α N-catenin (goat, Santa Cruz, sc-1498, 1:500), GFP (Invitrogen, rabbit, A11122, 1:1000), GAPDH (mouse, Kangcheng, KC-5G4, 1:5000).

Statistics

Statistical tests were carried out using GraphPad Prism 5 (GraphPad software). Unless otherwise stated, two-tailed Student's *t*-test (for sample pairs) or one-way ANOVA (for 3 or more conditions) followed by Tukey's multiple comparison tests were used. For experiments with two independent variables, two-way ANOVA followed by Bonferroni post-tests were used, between conditions at the same time point or in the same spine subtype. For PSA analysis in cultured neurons, repeated measure ANOVA, followed by Tukey's multiple comparison tests was used. For comparison of inter-spine distance distribution, the Kolmogorov-Smirnov two-sample-test was used. Linear regressions were performed in GraphPad Prism 5. Data distribution was assumed to be normal although not formally tested. Results are shown as mean \pm SEM, and "n" refers to either the number of neurons (for morphological analysis), the number of animals (for western blots) or the number of spines/spine pairs (for spine length/width/inter-spine distance measurements and PSA). Sample sizes were predetermined using web-based sample size/power calculator (<http://stat.ubc.ca/~rollin/stats/ssize/n2.html>) and are similar to those reported in our previous publications (Tan et al., 2010; Zheng et al., 2014) and other publications in the field (Chen et al., 2012; Chung et al., 2013; Erturk et al., 2014; Fu et al., 2012; Kwon and Sabatini, 2011; Lai et al., 2012; Mikuni et al., 2013; Parkhurst et al., 2013). All data analyses were performed blinded to the experimental condition. All conditions statistically different from control are indicated. * $P < 0.05$; ** $P < 0.01$; *** $P < 0.001$.

Supplemental References

- Abel, T., Nguyen, P.V., Barad, M., Deuel, T.A., Kandel, E.R., and Bourtchouladze, R. (1997). Genetic demonstration of a role for PKA in the late phase of LTP and in hippocampus-based long-term memory. *Cell* 88, 615-626.
- Ashby, M.C., Maier, S.R., Nishimune, A., and Henley, J.M. (2006). Lateral diffusion drives constitutive exchange of AMPA receptors at dendritic spines and is regulated by spine morphology. *J Neurosci* 26, 7046-7055.
- Belichenko, P.V., Masliah, E., Kleschevnikov, A.M., Villar, A.J., Epstein, C.J., Salehi, A., and Mobley, W.C. (2004). Synaptic structural abnormalities in the Ts65Dn mouse model of Down Syndrome. *J Comp Neurol* 480, 281-298.
- Bian, W.J., Miao, W.Y., He, S.J., Wan, Z.F., Luo, Z.G., and Yu, X. (2015). A novel Wnt5a-Frizzled4 signaling pathway mediates activity-independent dendrite morphogenesis via the distal PDZ motif of Frizzled 4. *Dev Neurobiol* 75, 805-822.
- Brault, V., Moore, R., Kutsch, S., Ishibashi, M., Rowitch, D.H., McMahon, A.P., Sommer, L., Boussadia, O., and Kemler, R. (2001). Inactivation of the beta-catenin gene by Wnt1-Cre-mediated deletion results in dramatic brain malformation and failure of craniofacial development. *Development* 128, 1253-1264.
- Chen, J.L., Villa, K.L., Cha, J.W., So, P.T., Kubota, Y., and Nedivi, E. (2012). Clustered dynamics of inhibitory synapses and dendritic spines in the adult neocortex. *Neuron* 74, 361-373.
- Chubykin, A.A., Atasoy, D., Etherton, M.R., Brose, N., Kavalali, E.T., Gibson, J.R., and Sudhof, T.C. (2007). Activity-dependent validation of excitatory versus inhibitory synapses by neuroligin-1 versus neuroligin-2. *Neuron* 54, 919-931.
- Chung, W.S., Clarke, L.E., Wang, G.X., Stafford, B.K., Sher, A., Chakraborty, C., Joung, J., Foo, L.C., Thompson, A., Chen, C., *et al.* (2013). Astrocytes mediate synapse elimination through MEGF10 and MERTK pathways. *Nature* 504, 394-400.
- Erdmann, G., Schutz, G., and Berger, S. (2007). Inducible gene inactivation in neurons of the adult mouse forebrain. *BMC Neurosci* 8, 63.
- Erturk, A., Wang, Y., and Sheng, M. (2014). Local pruning of dendrites and spines by caspase-3-dependent and proteasome-limited mechanisms. *J Neurosci* 34, 1672-1688.
- Fu, M., Yu, X., Lu, J., and Zuo, Y. (2012). Repetitive motor learning induces coordinated formation of clustered dendritic spines in vivo. *Nature* 483, 92-95.
- Goebbels, S., Bormuth, I., Bode, U., Hermanson, O., Schwab, M.H., and Nave, K.A. (2006). Genetic targeting of principal neurons in neocortex and hippocampus of NEX-Cre mice. *Genesis* 44, 611-621.
- Harada, N., Tamai, Y., Ishikawa, T., Sauer, B., Takaku, K., Oshima, M., and Taketo, M.M. (1999). Intestinal polyposis in mice with a dominant stable mutation of the beta-catenin gene. *EMBO J* 18, 5931-5942.
- Harris, K.M., Jensen, F.E., and Tsao, B. (1992). Three-dimensional structure of dendritic spines and synapses in rat hippocampus (CA1) at postnatal day 15 and adult ages: implications for the maturation of synaptic physiology and long-term potentiation. *J Neurosci* 12, 2685-2705.
- He, S., Ma, J., Liu, N., and Yu, X. (2010). Early enriched environment promotes neonatal GABAergic neurotransmission and accelerates synapse maturation. *J Neurosci* 30,

7910-7916.

- Hirani, N., Westenberg, M., Gami, M.S., Davis, P., Hope, I.A., and Dolphin, C.T. (2013). A simplified counter-selection recombineering protocol for creating fluorescent protein reporter constructs directly from *C. elegans* fosmid genomic clones. *BMC Biotechnol* 13, 1.
- Kim, S.A., Tai, C.Y., Mok, L.P., Mosser, E.A., and Schuman, E.M. (2011). Calcium-dependent dynamics of cadherin interactions at cell-cell junctions. *Proc Natl Acad Sci U S A* 108, 9857-9862.
- Kwon, H.B., and Sabatini, B.L. (2011). Glutamate induces de novo growth of functional spines in developing cortex. *Nature* 474, 100-104.
- Lai, C.S., Franke, T.F., and Gan, W.B. (2012). Opposite effects of fear conditioning and extinction on dendritic spine remodelling. *Nature* 483, 87-91.
- Lin, J.Y., Lin, M.Z., Steinbach, P., and Tsien, R.Y. (2009). Characterization of engineered channelrhodopsin variants with improved properties and kinetics. *Biophys J* 96, 1803-1814.
- Lu, W., Shi, Y., Jackson, A.C., Bjorgan, K., During, M.J., Sprengel, R., Seuberg, P.H., and Nicoll, R.A. (2009). Subunit composition of synaptic AMPA receptors revealed by a single-cell genetic approach. *Neuron* 62, 254-268.
- Miesenbock, G., De Angelis, D.A., and Rothman, J.E. (1998). Visualizing secretion and synaptic transmission with pH-sensitive green fluorescent proteins. *Nature* 394, 192-195.
- Mikuni, T., Uesaka, N., Okuno, H., Hirai, H., Deisseroth, K., Bito, H., and Kano, M. (2013). Arc/Arg3.1 is a postsynaptic mediator of activity-dependent synapse elimination in the developing cerebellum. *Neuron* 78, 1024-1035.
- Nagai, T., Ibata, K., Park, E.S., Kubota, M., Mikoshiba, K., and Miyawaki, A. (2002). A variant of yellow fluorescent protein with fast and efficient maturation for cell-biological applications. *Nature Biotechnol* 20, 87-90.
- Park, C., Falls, W., Finger, J.H., Longo-Guess, C.M., and Ackerman, S.L. (2002). Deletion in Catna2, encoding alpha N-catenin, causes cerebellar and hippocampal lamination defects and impaired startle modulation. *Nat Genet* 31, 279-284.
- Parkhurst, C.N., Yang, G., Ninan, I., Savas, J.N., Yates, J.R., 3rd, Lafaille, J.J., Hempstead, B.L., Littman, D.R., and Gan, W.B. (2013). Microglia promote learning-dependent synapse formation through brain-derived neurotrophic factor. *Cell* 155, 1596-1609.
- Saglietti, L., Dequidt, C., Kamieniarz, K., Rousset, M.C., Valnegri, P., Thoumine, O., Beretta, F., Fagni, L., Choquet, D., Sala, C., *et al.* (2007). Extracellular interactions between GluR2 and N-cadherin in spine regulation. *Neuron* 54, 461-477.
- Schoonover, C.E., Tapia, J.C., Schilling, V.C., Wimmer, V., Blazeski, R., Zhang, W., Mason, C.A., and Bruno, R.M. (2014). Comparative strength and dendritic organization of thalamocortical and corticocortical synapses onto excitatory layer 4 neurons. *J Neurosci* 34, 6746-6758.
- Sharma, K., Fong, D.K., and Craig, A.M. (2006). Postsynaptic protein mobility in dendritic spines: long-term regulation by synaptic NMDA receptor activation. *Mol Cell Neurosci* 31, 702-712.
- Shi, S., Hayashi, Y., Esteban, J.A., and Malinow, R. (2001). Subunit-specific rules governing AMPA receptor trafficking to synapses in hippocampal pyramidal neurons.

- Cell 105, 331-343.
- Tai, C.Y., Mysore, S.P., Chiu, C., and Schuman, E.M. (2007). Activity-regulated N-cadherin endocytosis. *Neuron* 54, 771-785.
- Tan, Z.J., Peng, Y., Song, H.L., Zheng, J.J., and Yu, X. (2010). N-cadherin-dependent neuron-neuron interaction is required for the maintenance of activity-induced dendrite growth. *Proc Natl Acad Sci U S A* 107, 9873-9878.
- Wallace, W., and Bear, M.F. (2004). A morphological correlate of synaptic scaling in visual cortex. *J Neurosci* 24, 6928-6938.
- Woolley, C.S., and McEwen, B.S. (1993). Roles of estradiol and progesterone in regulation of hippocampal dendritic spine density during the estrous cycle in the rat. *J Comp Neurol* 336, 293-306.
- Yu, X., and Malenka, R.C. (2003). Beta-catenin is critical for dendritic morphogenesis. *Nat Neurosci* 6, 1169-1177.
- Zagrebelsky, M., Holz, A., Dechant, G., Barde, Y.A., Bonhoeffer, T., and Korte, M. (2005). The p75 neurotrophin receptor negatively modulates dendrite complexity and spine density in hippocampal neurons. *J Neurosci* 25, 9989-9999.
- Zhang, X., and Poo, M.M. (2002). Localized synaptic potentiation by BDNF requires local protein synthesis in the developing axon. *Neuron* 36, 675-688.
- Zhang, Y.P., and Oertner, T.G. (2007). Optical induction of synaptic plasticity using a light-sensitive channel. *Nature Methods* 4, 139-141.
- Zheng, J.J., Li, S.J., Zhang, X.D., Miao, W.Y., Zhang, D., Yao, H., and Yu, X. (2014). Oxytocin mediates early experience-dependent cross-modal plasticity in the sensory cortices. *Nat Neurosci* 17, 391-399.